Universidad Autónoma del Estado de México

Doctorate Program on Engineering Sciences

Dynamic Systems and Control

Development, modeling and control of an adjustable stiffness-based supination-pronation forearm physical rehabilitator

THESIS

by

M. en I. Adrian Camacho Ramirez

Advisors:
Dr. Juan Carlos Ávila Vilchis
Dra. Adriana H. Vilchis-González
Dra. Belem Saldivar Márquez

Toluca, Estado de México. February 2023

Contents

List of Figures

List of Tables

Acronyms

ROM Range of motion

ODEs Ordinary differential equations

PID Proportional, integral, derivative

STA Super-twisting algorithm

SOSM Second-order sliding mode

INEGI Instituto Nacional de Estadística y Geografía

PWM Pulse width modulation

RCP Rapid control prototyping

ADC Analog to digital converter

PLA Polyactic acid

ADL Activities of daily living

DOF Degree of freedom

SMC Sliding mode controller

ASM Asymptotic sliding mode

ST Super-twisting

VGSTA Variable gain super-twisting algorithm

PD Proportional-derivative

TA Tension adjustment

Chapter 1

Introduction

Wrist and forearm therapy exercises, which include bending (flexion and extension), turning the forearm over (supination and pronation), hand gripping exercises, and forearm strengthening with a dumbbell, these exercises are important to build strength and operation for the wrist, hand, elbow, and shoulder.

Assisted motor therapy as continuous passive motion devices is used during the first phase of rehabilitation and plays a critical role in improving passive motion in a specific plane of movement, and protecting the healing process of the tissue, however, current devices are unable to recreate these exercises well. The current thesis is aimed to design and examine the viability of a wrist-forearm exercise device that reproduces pronation-supination range of motion (ROM) therapy and improves the strength of the associated muscles, by adopting an adjustable stiffness system. The device incorporates a handle that will serve as a guide for the required movements linked with two springs to provide stiffness and a smooth return, and four non-elastic cables actuated for two linear actuators that provide linear motion.

1.1 Background

Mechanisms with elastic joints are a research topic in the robotics community due to desired robot skills such as fine manipulation, sensitivity for gentle interaction with the environment, and controlled movements when the system interacts with humans in direct physical contact [10–12]. systems that have these characteristics are described below.

A tensegrity system is a state of stable self-balance structure, consisting of a discontinuous set of elements working under compression and a continuous set of elements working under tension [13]. This type of system has different design possibilities with advantages in strength, lightness, and the economy of materials. Richard Buckminster Fuller coined the term *tensegrity* [14], which is formed from the contraction of two words *tensional integrity*. This means that the elements subjected to a tension that constitutes the structure are responsible for generating a unique form for giving it balance, an example of this kind of system is seen in Fig. 1.1.

The great advantage of tensegrity systems is that their configuration stability depends only on the set of flexible elements jointly with the rigid elements without the intervention of an external force [1].

In the last few years, cable-driven systems have been intensively discussed in the robot society as a hot topic of robotics research. These systems have some characteristics, such as lightness, large workspace, low cost, high-speed movement if required, and ease to build [15]. Cable-driven robots can be considered for applications where it is necessary to modify pre-stress levels by changing cable lengths. This adjustment generates a new configuration form creating a modification in its stiffness. In [16] suggests that designing a control strategy that can control position and stiffness at the same time in these types of systems is difficult to achieve.

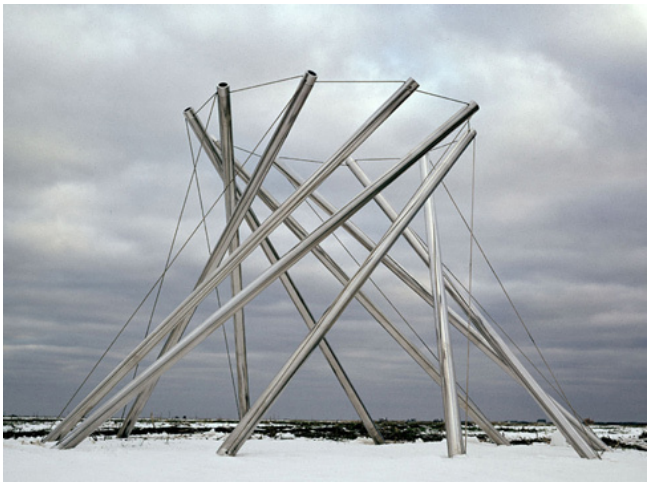

Figure 1.1: Tensegrity structure V-X by Kenneth Snelson, 1968.

The configuration characteristics of soft robotics include applications in biomechanics such as manipulators and human-based robotic systems [17]. Mechanical design, manufacture, analysis, modelling, and control are major challenges to be addressed. The possibilities of generating a unique form of structure, motion, reconfiguration, and mechanical simplicity are greater with an adjustable stiffness system. Taking advantage of these properties an application for human upper limb rehabilitation is desired.

1.2 Objective

1.2.1 General Objective

Analyze and design a variable stiffness system that can recreate wrist-forearm therapy exercises without or with minimal intervention of a physical therapist, in order to build a mathematical model that represents their behavior and synthesize a control law that allows the system to perform the supination-pronation rehabilitation protocols.

1.2.2 Specific Objective

- Analyse the kinematics, statics, and dynamics.
- Define the system workspace.
- Establish the relationships that have certain configurations and tension variations with the end-effector in the workspace to perform the desired phase of therapy.
- Design a control law that allows modifying the position and stiffness of the system.
- Perform experiments using a platform with a geometric configuration suitable for the proposed application.

1.3 Hypothesis

Rehabilitation protocols that are validated by specialists (doctors and physical therapists) can be executed by a variable stiffness device working in closed-loop configurations while minimizing structural and tracking errors.

The variable stiffness device allows modifying the position and stiffness through a series of cables, springs, and linear motors, applying external forces (patient) to this device can perform passive, active-assisted, and active rehabilitation movements throughout the entire range of motion.

1.4 Problem statement

One of the great problems of engineering is to generate theories, methodologies for design and analysis, and the field of rehabilitation robotics is not an exception. Studie these problems promise to be a source of interesting and incredible possibilities, concretely in the field of engineering and particularly in bioengineering, it would mean providing an alternative source of systems design presented in robotics such as unconventional mechanical platforms, manipulators, sensors, and actuators.

Based on what has been established, this project focuses on the development of a mathematical model of a variable stiffness device and on the synthesis of a control strategy that will allow the system to achieve desired objectives.

1.5 Motivation

Due to multiple applications that can involve variable stiffness systems, this project has put great interest in the physical rehabilitation that a person develops when trying to recover the condition or state that lost, due to an illness, accident, or other types of health disorder.

An approach aimed at promoting and achieving certain levels of rehabilitation on specific parts of the body can be based on the characteristics of the human bones and tendons because they are connected in such a way that enables easy control of movement. As shown in [18] the bones give a compressing load capacity and the tendons have the ability to stabilize the body in certain configurations. Figure 1.2 and Fig. 1.3 show how tendons are attached to the different parts of the bones to be able to control them.

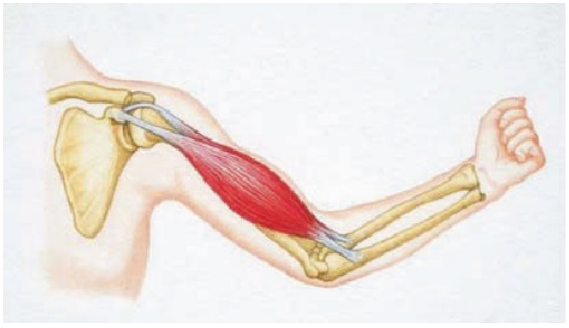

Figure 1.2: Arm joint and elbow joint [1].

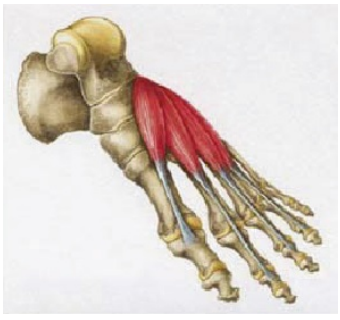

Figure 1.3: Toes joint [1].

Because movement is an integral part of human life and animal life, we want to simulate a more natural human movement, this adjustable stiffness device moves as a single unit and the tension in one of its members runs through the entire structure, we can take advantage of this quality where these structures can move more fluently from one configuration to another [19].

An example in which a device can be seen as a stiffness structure is the hand posture corrector for the rehabilitation of the dynamic orthosis of the finger and wrist, it is shown in Fig. 1.4, which represents an essential tool for therapists who treat patients recovering from tennis elbow, tendonitis in the wrist, stroke effects, various hand traumas, among many others. Another example is the MariBot 5 (see Fig 1.5) which is a cable-suspended rehabilitation robot,

in which the arm can be suspended on a surface with straps attached by cables, those cables control the movement by changing lengths through pulleys and three motors [3].

Figure 1.4: Dynamic hand splint [2].

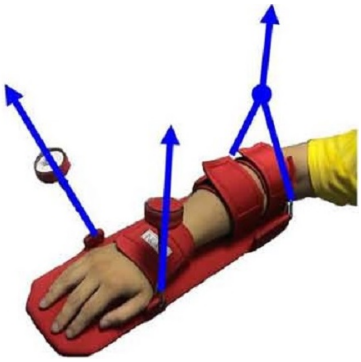

Figure 1.5: MariBot 5 [3].

This thesis is organized as follows. Chapter 2 shows the desirable features that the rehabilitation device must have like modeling, control, and construction. Chapter 3 reviews the existing literature on automatic rehabilitation devices and presents the state-of-the-art wrist-forearm rehabilitation system. Chapter 4 gives electronic and mechanical information about the components used to control the rehabilitator. Chapter 5 presents the adjustable stiffness rehabilitation device, the control strategies for tracking, and tension adjustment. Experimental results that show the performance of the developed device are presented in Chapter 6, conclusions are found at the end of the thesis, and results of a published article, a submitted article, and an experimental platform are shown in appendix.

Chapter 2

Theoretical background

2.1 Static and kinematic determination

A structure is statically determined if the equilibrium equations are sufficient to find the internal forces and structure's displacements, subject to the action of external loads [20]. On the other hand, a structure is statically indeterminate if it has more elements than the minimum necessary to guarantee the solution of the equilibrium equations, consequently admits more than one solution. This also implies that the structure may contain prestressing forms and its elements may be stressed even in the absence of external loads [21].

A structure is kinematically determined if any movement of translation or rotation of the assembly corresponds to a rigid element, in other words, it is required to add energy to the system to change its geometry. But if the structure is kinematically undetermined, there may be variations of the geometry without external forces inserting energy into the system [22].

The structure is called self-stressed if it can generate initial stress in its elements in the absence of external forces and fixed nodes. When rigid elements make an assembly or structure, the choice of lengths of the elements and their connectivity can cause the structure geometry is defined by a single set of coordinates of the nodes. If a change in the geometry doesn't produce any variation in the length of the elements, the mechanism is known as *finite*, and if a change in the geometry produces infinitesimal variations the mechanism is known as *infinitesimal* [13].

2.2 Dynamic analysis

A structure is statically determined if the equilibrium equations are sufficient to find the internal forces and structure's displacements, subject to the action of external loads [20]. On the other hand, a structure is statically indeterminate if it has more elements than the minimum necessary to guarantee the solution of the equilibrium equations, consequently admitting more than one solution. This also implies that the structure may contain prestressing forms and its elements may be stressed even in the absence of external loads [21].

A structure is kinematically determined if any movement of translation or rotation of the assembly corresponds to a rigid element, in other words, it is required to add energy to the system to change its geometry. But if the structure is kinematically undetermined, there may be variations of the geometry without external forces inserting energy into the system [22].

The structure is called self-stressed if it can generate initial stress in its elements in the absence of external forces and fixed nodes. If a change in the geometry doesn't produce any variation in the length of the elements, the mechanism is known as *finite*, and if a change in the geometry produces infinitesimal variations the mechanism is known as *infinitesimal* [13].

2.3 Tensegrity

The term tensegrity has been described as a class of self-stressed systems defined as a set of compressed solid elements (bars) in a set of tensioned elements (cables) [13]. The tensioned elements drastically modified following a specific direction through an external agent within the prestressed cables [21].

With some advantages like storing energy when they deform and releasing when they return to their original form, compact, volume, lightness, structural and geometric efficiency [13]. Due to their characteristics, tensegrity systems have had a great interest in several applications such as mobile robots [23], deployable systems [24], and manipulators [25]. The distribution of forces in tensegrity robots has been lately studied mostly for exploration [26], where it is shown that force distribution is a robust and reliable robot property in interaction with the environment, landing, and exploration.

One of the tensegrity structures problems is to find an initial configuration, this method called *form-finding* is the process that allows finding a feasible initial geometric configuration, generally in the absence of external loads. Theoretical methods take into account only geometric parameters while others, additionally take force parameters, use virtual models for approving valid and balanced topologies, and even a trial and error method is also considered as a configuration search process. A review of several methods of form-finding is shown in [27].

Some tensegrity robots have been planned to help and perform medical assistance in rehabilitation. They can supplies medicine if these robots are provided with certain mobility skills [28]. Or to complete physical rehabilitation, in [29] a portable robot *exosuit* can offer its user's stability and strength, designed to act in conjunction with the user's movements (see Fig. 2.1).

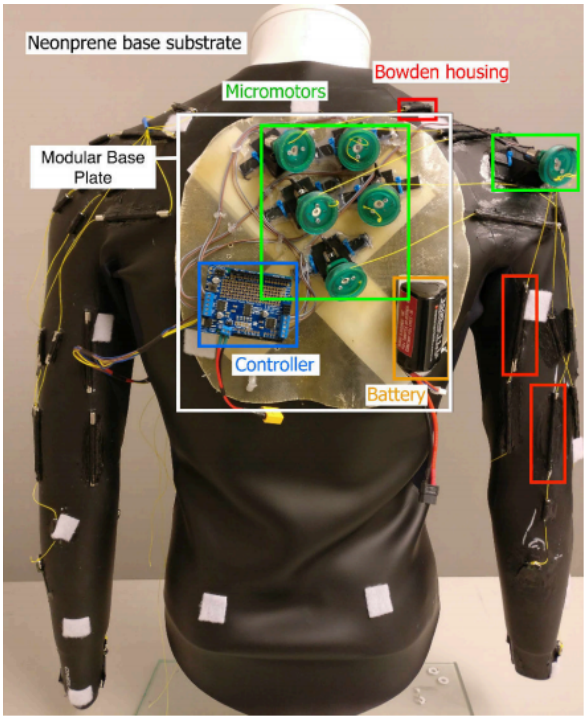

Figure 2.1: Crux: system components [4].

Despite the great advantages and variety of applications, only a few cable-driven tensegrity robots have been developed. Among the reasons we can include:

- Cable-driven tensegrity robots are mechanically complicated and demanding to build.

- Design requirements vary from conventional robots (exoskeleton, soft, cable-driven, articulated, etc) and traditional mechanisms.
- Due to the change of position and forces on the robot to change the configuration, the control becomes more complex.
- There are no standard components to build a cable-driven tensegrity robot.

2.4 Cable-driven robot

In the last few years, parallel cable-driven robots have attracted attention in the rehabilitation robotics community due to their characteristics of lightness, high reconfiguration speed, flexibility in movements, and low cost compared to other robots such as exoskeletons [30]. Because of these characteristics, some applications have been developed as astronomical observation, construction devices, rescue, service, and rehabilitation [3, 31].

In [3] presents a cable-driven robot of 3 degrees of freedom for human rehabilitation of the upper limb (see Fig. 2.2), which consists of a set of cables driven by motors, the arm is fastened onto a splint. The cables are connected to the upper limb, controlling the length of the cables so the rehabilitation treatment can be performed under a defined path. A light inherently safe robotic system to assist the movement of a person in recovery and training therapy, where the concept establishes the idea of a suspended puppet using cables that control posture, balance, and motor functions is presented in [31].

Figure 2.2: NeReBot [3].

Cable-driven with stress manipulation are now considered for several applications for their reconfiguration qualities and lightness. Moreover, When the lengths of the cables are modified, the stiffness of the system can change, which modifies the pre-stress level in the mechanism [21].

Control schemes that deal with configuration changes and stiffness variation at the same time have not been developed in the literature [16]. The control of this kind of mechanism is tedious because the cables need to be under constant stress. This constraint is very important

because positive tension must be ensured to avoid negative tension in the cables. A modulation in a range of tension is of great interest to vary the system stiffness [16].

2.5 Modeling

The most common formulation uses ordinary differential equations (ODEs) with the help of the Euler-Lagrange equation. Numerous developed control algorithms are based on this type of differential equation. The equation of motion can be derived from Lagrangian equations, where features are provided by rigid bodies, cables, gravity, mass, internal forces, external forces, and friction forces on the elements.

2.6 Control

Skelton and Sultan [32] showed that the elements to be driven could be rigid, cables, or a combination of both, where linear controls are the most used. Active control and estimation problem based on tracking are discussed in [33] using sensors and actuators in a multibody agent where the controller is designed with a time-varying relative formation of all the robots. In [16] two control strategies are implemented in a tensegrity mechanism driven by cables in order to convert it into a variable stiffness device. Its goal is to introduce a control strategy for position and stiffness control. The first strategy influenced for the cable-driven control, uses a tension distribution algorithm. The second proposal is a speed distribution algorithm, where an angular velocity of the final effector is generated.

It is possible to use motors with a series of pulleys to modify the lengths of all the cables individually assured by a control algorithm. A superior approach is to examine the desired position, force, or torque for the motor or some point of the end effector. As shown in [34] a robust closed-loop PID controller is proposed, analyzed through the direct method of Lyapunov, the controller's gains are proposed with correction terms based on the null space of the Jacobian matrix.

In [35] assume that the cables of the robot are actuated, this means there are two control variables: the length of the cable and its tension. To incorporate both, a distributed form of impedance control is used. The control provides adjustable stiffness through the change of gains the tensions are controlled by a PD controller on the DC motor.

Many of the controllers developed in the literature are highly dependent on the exact system's mathematical model. The variances between the real system and the mathematical model may be due to un-modeled dynamics and unknown or variations of parameters, which makes the model being too complicated. For these reasons, the use of robust control [36, 37] seeks to solve this problem, despite such system/model mismatches. An option for this controller is the super-twisting algorithm (STA), which is a robust second-order siding mode (SOSM), where the design of the sliding surface depends on the measurement of speed and position but not on knowing exactly the parameters of the system [38, 39]. The STA guarantees robustness regarding to modeling mistakes and external disturbances while reducing the unwanted phenomenon of high-frequency oscillations (chattering) which is the main problem by the first-order sliding mode based on the sign function [40]. Finite-time convergence and stability are proved with a Lyapunov function [41–43], the stability analysis of the proposed controller for the rehabilitation system has been aimed in the same way.

Since the main idea is to change the speed and position of the actuators when the desired structure configuration change, there is no explicit control law that provides that [44].

2.7 Rehabilitation protocols

The purpose of this rehabilitator is to perform a movement that allows performing one of the techniques of exercise therapy for the human upper limb. The movements used in treatment may be classified as follows [45]:

Passive Movement: limbs motion without the effort of the person. The motion conducted by a therapist, automatic device or machine, is carried out to a segment of the body, muscle or joints, classified as:

- Relaxed movements without effort or pain.
- Passive mobilization techniques (oscillatory, maintained and manipulative).

Active Movement: a type of movement performed by voluntary contraction and physical effort exerted into muscular activity, classified as:

- **Assisted:** A therapist or an automatic device helps or compensates to regain muscle strength and coordination of the patient's injured limb.
- **Free:** The working muscles are subject only to the forces of gravity with objects such as medicine balls, dumbbells, sand bags or any other objects that aren't attached to anything.
- **Assisted-Resisted:** With the use of resistance bands or tubing help the muscles work against resistance forces, with the help of objects such as resistance bands.
- **Resisted:** The forces of resistance make the muscle systematically gain strength and endurance.

The human upper limb consists in three main articulations: shoulder, elbow and wrist. Where the daily task range of motion are shown in Table 2.1.

Table 2.1: Shoulder, elbow and wrist range of motion [6].

Joint	Movement	Range (AO)	Range (AAOS)
Shoulder	Abduction	0-160°/180°	0-180°
	Adduction	0-30°	0°
	Flexion	0-150°/170°	0-180°
	Extension	0-40°	0-60°
	External rotation	0-70°	0-90°
	Internal rotation	0-70°	0-70°
Elbow	Flexion	0-150°	0-150°
	Extension	0-10°	0°
	Pronation	0-90°	0-80°
	Supination	0-60°	0-80°
Wrist	Flexion	0-50°	0-80°
	Extension	0-35°/70°	0-70°
	Radial deviation	0-25°/30°	0-20°
	Ulnar deviation	0-30°/40°	0-30°

Rehabilitation therapy is commonly performed for six weeks and begins with active movements without pain in the ROM of the wrist and forearm. Once patients reach approximately 90% of the range of motion, progressive strengthening can be executed by:

- Isometric exercises.
- Elastic bands and tubing.
- Rehabilitation equipment.

Rehabilitation time depends on how intense and how often the therapeutic exercises are performed. Physical therapy consists of 3 main stages of rehabilitation: passive, active-assisted, and active [5, 46]. In the passive stage, a therapist helps the patient to mobilize the affected limb along the corresponding ROM, the patient does not make any effort and only seeks to gain mobility throughout the range. In the active-assisted stage, the exercises are performed by the patient himself, but he can have help from the therapist when he needs it. Some strength exercises begin to be performed. In active exercises, the patient already performs the movements and exercises without any external help, in this stage the aim is to gain muscle and endurance. When using a device, the following general guidelines are recommended in [5,47,48] for proper upper limb rehabilitation.

Stage 1. Instantaneous Motion (Passive)

Movements of the forearm and wrist are made along the ROM without the patient having pain in the limb with the goal to avoid muscular atrophy. The exercises performed are with the help of the therapist and it is recommended to perform 10-min series. The patient should avoid lifting or carrying any heavy object at this stage. Once the pain and inflammation have almost completely disappeared, the procedure starts with the passive mobilization phase. Here, the physiotherapist will be in charge of performing the movements of flexion, extension, and radial and ulnar deviations. This work should be done painlessly or with a pain tolerable by the patient. A supination-pronation example exercise is shown in Fig. 2.3 where the therapist grasp the path motion is a rolling of the radius around the ulna at the distal radius.

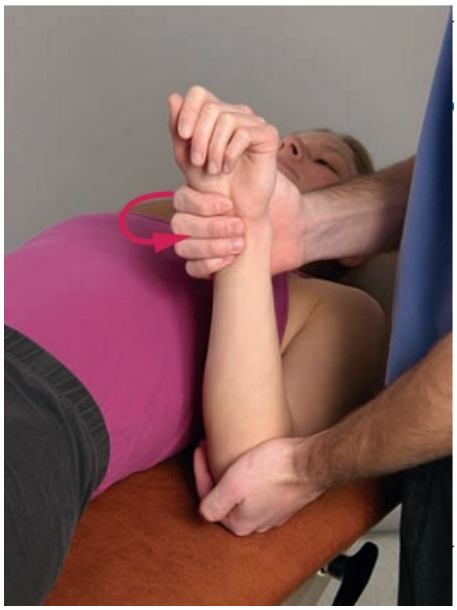

Figure 2.3: Forearm pronation [5].

Stage 2. Intermediate (Active-assisted)

Approximately after a month and a half after having recovered the ROM as it was before the injury, such movements are performed without the help of the therapist. Exercises are

performed with or without the help of the therapist or some device with the aim of gaining muscle and endurance with weights ranging from 1 lb to 2 lb.

Stage 3. Strengthening (Active)

Aside from the movements, depending on the pathology to be recovered, subsequently, the wrist-forearm mobilizations are carried out by the patient, along with the stretches that the physiotherapist will teach the patient. After two months, more intense exercises are performed with weights from 2 lb to 4 lb, weights or similar objects can be used, as well as resistance bands or tubes. Besides, functional movements such as exercises are performed where the wrist-forearm movement is fixed against a hard, unrelenting surface. In this stage, it can be used a small bar with weight for strengthening the affected forearm (see Fig. 2.4).

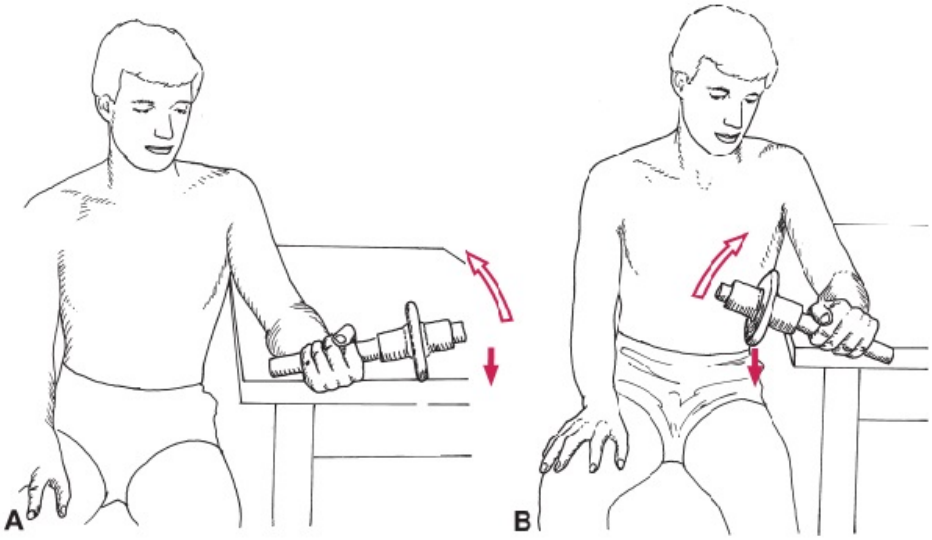

Figure 2.4: Mechanical resistance exercise (A) pronation and (B) supination [5].

Chapter 3

State of the art

3.1 Rehabilitation

According to the statistics of the INEGI, there are about 126 million people in Mexico in 2020. Of these, almost 5.7% reports having significant difficulty or not being able to do any of the basic activities and about 15.9 million have mild or moderate difficulties in carrying out the same activities [9]. Globally, about 190 million adults experience some degree of disability, and it is calculated that over 90 million children under 15 years old live with a moderate or severe disability [49].

There are several causes of disability that range from congenital, some accident, or advanced age, these being the main causes [50]. Of this population, the percentage with disabilities, by type of disability according to the 2015 age group, is given in Tab. 2.1.

Table 3.1: Kinds of disability [9].

Kind od disability / Range of age	0-14	15-29	30-59	60 and more
Walk, raise o lower using their legs	36.2	32.1	56.2	81.3
See	26.9	44.6	58.2	67.2
Move or use arm and hand	14.1	18.2	28.5	42.7
Learning, remember or focus	40.8	31.5	32.1	44.6
Listening	13.4	18.5	24.2	46.9
Speak or communicate	26.6	28.0	20.1	16.3

Based on the exercises during different rehabilitation sessions, and on the types of movements of the upper limb supervised by specialist therapists, the following exercises are identified:

- Series of excluding exercises by articulation.
- Exercise with an apparent load.
- Activation of muscle memory through trajectory tracking.

In order to have adequate physical rehabilitation, it is necessary for a physical therapist to attend to the patient, but since physical therapies are time-consuming and require several sessions, the existing therapists are not enough to meet the emerging demand of patients. [51]. Given this situation, the development and construction of automatic devices that meet these needs are required, which would cause an increase in the number of training sessions for a

patient with consistent repetitions and enable the possibility that one therapist to prepare two or more patients at once [52].

Different studies have shown that intensive and repetitive therapy exercises with adequate duration and consistency, significantly improve motor skills [53, 54]. Rehabilitation based on virtual reality significantly reduces the deterioration of the affected limb and improves motor function allowing recovery [55, 56]. Motor learning is crucial in rehabilitation with ADL or games, motor coordination is improved, muscle memory is recovered, and the muscles begin to gain strength and endurance [57, 58]. Patient active participation is crucial for increasing robotic rehabilitation efficacy. In the impedance-admittance control technique, the patient's participation is very active, this allows rehabilitation to be more effective since the patient notices his progress [59]. Robot-assisted therapy proposed in [60] restore loss of motor function when physical training is repetitive, intense, and quantifiable.

Although exist rehabilitation robots, they are still not enough to cover the increasing demand and those that are in stock are expensive, heavy, require large workspace, they do not provide information in real-time to both the patient and the therapist about the movements performed. The past decades have seen a vast development of rehabilitation robots. Some robotic therapy devices for the upper limb are typically complex, heavy, and expensive, and the design can be tedious. In [61] shows the evolution of the rehabilitation robots, in addition, the current state of clinical evidence is reviewed.

3.2 Overview of upper limb rehabilitation robot

Upper-limb robotic devices are divided into two categories: prosthesis and orthosis. A prosthesis is a functional replacement for replacing or augmenting a missing or impaired limb. An orthosis is a device made to support, align, prevent, or correct deformities or to help someone move it more easily [62]. In particular, the orthoses can be divided into two categories: devices that use the end effector aligned with the user (i.e. hand, arm), and devices that have been made to mechanically align its joints with the joints of the user as the exoskeleton robots. An overview of automatic orthoses devices for upper limb rehabilitation is shown in Table 3.2.

A bimanual lifting rehabilitator [63], requires patients to lift a weight off the table with two hands, support it, then lower it on the table. MIT-MANUS [65] is configured to provide passive rehabilitation training for the elbow, forearm, and wrist. The training is through a series of tasks displayed on a monitor, providing sensorimotor rehabilitation. The purpose of the Arm Guide device [66] was to investigate the effects of rehabilitation robotics, proving that intense and repetitive active-assistive movements and exercises improve arm mobility after chronic stroke. GENTLE/S [67] is a rehabilitation device based on integrating appropriate haptic and virtual reality environments where passive and active-assisted tasks are performed. HandCARE [76] is a rehabilitation device that uses cables attached to each finger, where motors and pulleys allow force and displacement control, and each one of the five fingers has independent movement.

RUPERT is a robot driven by a pneumatic muscle [70] and [69], the robot provides training for activities of daily living (ADL) like reaching objects and feeding. CADEN-77 [71] driven by motors, cable-driven systems, and bearing is an exoskeleton with 7 DOF that assists upper limb rehabilitation, designed based on ADL movements. MAHI Exo II [72] with 3-DOF parallel mechanism focused on the forearm and wrist joints, designed for passive, assisted, and active rehabilitation, this design encloses the forearm in a bearing. MEDARM [73] consists of a robotic exoskeleton for improving motor function for the shoulder and elbow joints, the movements are driven by cables attached to motors, and the robot is mounted onto a support structure and a movable chair. ARMin II [74] enhances the outcome of neuromuscular rehabilitation, based on impedance and admittance control strategies, with five adjustable segments which allow it

Table 3.2: Overview of upper limb rehabilitation robots

Type	Device	DOFs	Part of Limb	Actuator mode	Control	Training mode
End-effector	The Bimanual Lifting [63]	1	Distal	Bimanual load lifting	Force	Active
End-effector	MIT MANUS [64, 65]	5	Distal	Motor	Impedance	Active & Passive
End-effector	Arm Guide [66]	3	Proximal and Distal	Motor	Impedance	Active & Passive
End-effector	GENTLE/S [67]	3	Proximal and Distal	Motor	Position	Passive
End-effector	HandCARE [68]	5	Distal	Motor	Force	Active
Exoskeleton	RUPERT [69, 70]	4	Proximal and Distal	Pneumatic	Force and Impedance	Active
Exoskeleton	CADEN-7 [71]	7	Proximal and Distal	Motor	Position	Passive
Exoskeleton	MAHI Exo II [72]	5	Distal	Motor	Position	Active
Exoskeleton	MEDARM [73]	6	Proximal and Distal	Line	Position	Passive
Exoskeleton	ARMin II [74]	7	Proximal	Motor	Force	Active & Passive
Exoskeleton	RiceWrist-S [75]	3	Distal	Motor	Force	Passive

to fit with different types of patients (sizes). The RiceWrist-S [75] is a robotic mechanism that uses ring bearings to surround the forearm that helps wrist flexion-extension and radial-ulnar deviation and forearm pronation-supination rehabilitation.

Various rehabilitation systems for different extremities have been created, as it was described for the upper limb in Table 2.2, where the exoskeletons that although they are a good option, their main disadvantage lies in the cost of the devices, as well as are available in some clinics or rehabilitation centers and also on occasions of their performance limitations or geometry.

One of the main problems with rehabilitation robots is that they must fit the patient in such a way that they do not suffer any injury or pain when performing the indicated movements or tasks. Both the parts and the mechanical joints of the robot must interact with their human counterpart comfortably, in other words, the robot must be ergonomic.

Chapter 4

Component selection and platform instrumentation

This chapter presents the considerations for the design of the adjustable stiffness device, as well as a detailed description of its characteristics and functions.

The design is aimed at people who require rehabilitation in the wrist-forearm, therefore the prototype of the device will be limited in its supination-pronation movement so that the development of the device's movement is more natural. The values of weights and dimensions of the elements should be the lightest possible so that the disabled person can use it without making an additional effort.

The adjustable stiffness device system objective is to give rehabilitation in pronation-supination ROM (see Fig. 4.1). The project considers the wrist-forearm range of motion, with passive and active movements, where the rehabilitating protocol is: stop all activity of the joint (or limit activity), i.e., rest and try to break the loop of more activity more injury (and more pain).

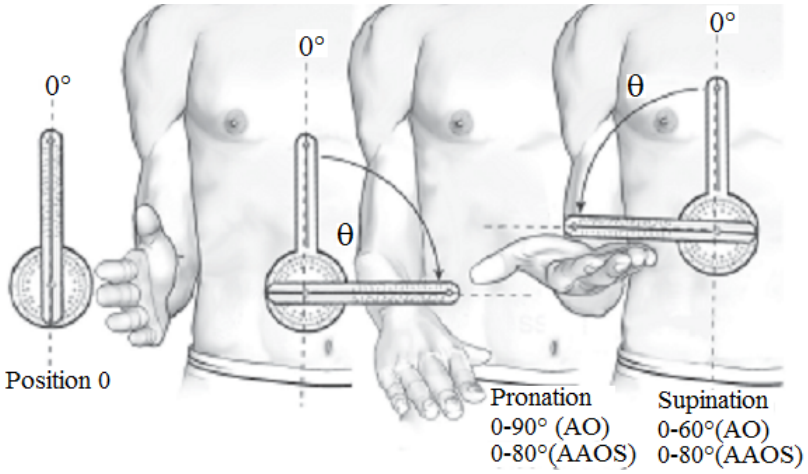

Figure 4.1: Normal values of pronation-supination movement [6].

4.1 Experimental setup

To demonstrate the effectiveness of the rehabilitator and the proposed control techniques, it was first verified by simulation with the Matlab & Simulink software with the mathematical model of the system and the proposed control laws. To validate the computed simulations in real-time, an experimental setup was created. This chapter shows how the experimental setup

was built, both in its mechanical and electrical components. An analysis of the key components such as the handle, the springs, and the motors is made.

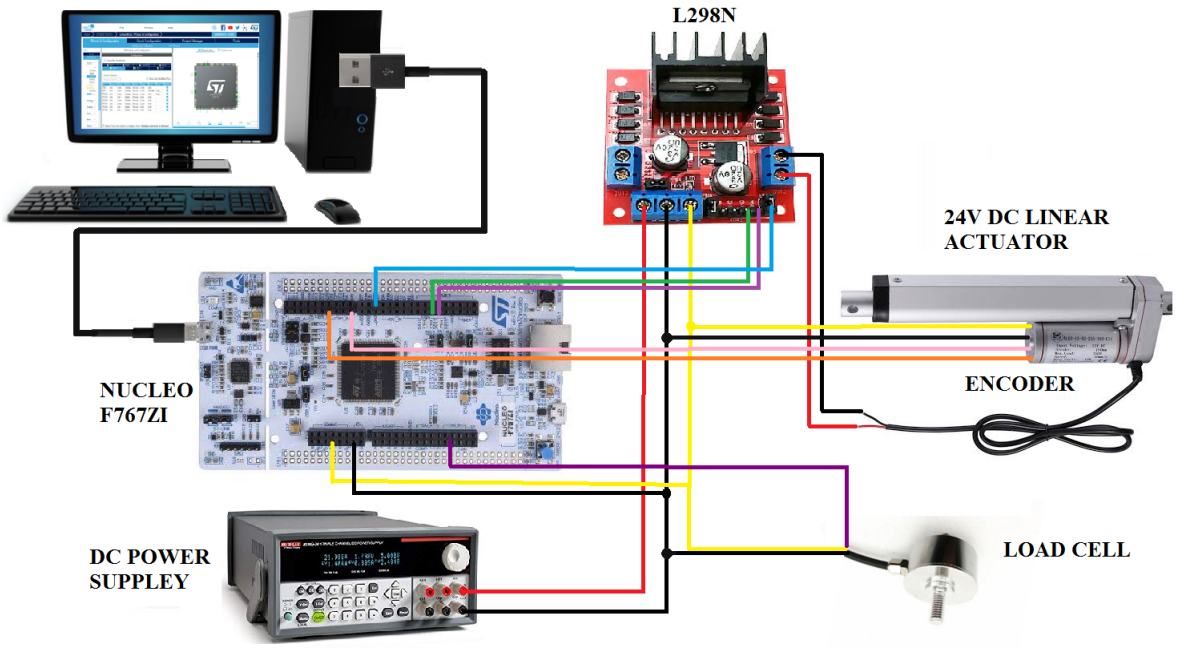

Figure 4.2: Schematics.

The experimental setup (see Fig. 4.2) used to verify the efficacy of the PID, PD, ASMC and STA controllers proposed in this project consists of the following components:

4.1.1 Linear actuator

The linear actuator TGA-Y-300-24-5-405 (see Fig. 4.3) is a type of lightweight and compact electric linear actuator, made of aluminum, takes DC motor element and gear reduction element and inner micro switch to stop the stroke automatically at the end and the beginning. This module adds an encoder to the original module of HF-TGA. An internal chip of encoder processed electric signal could recognize the stretching direction depending on its internal multiple photoelectric sensors and realize the visualization on controllable of stroke. Speed and load perform diagrams for the linear actuator are shown in Fig 4.4.

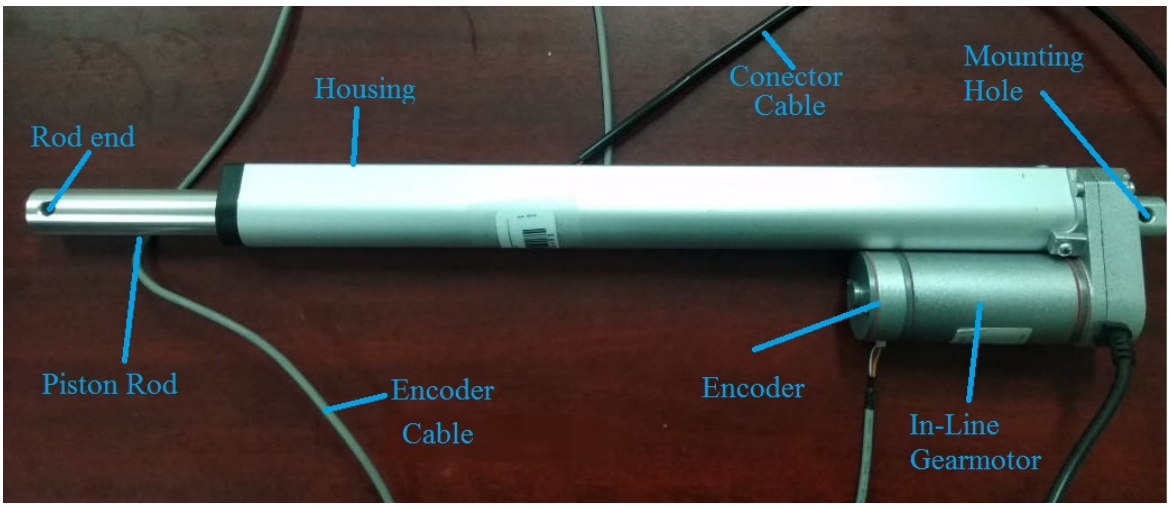

Figure 4.3: Linear Actuator.

The mechanical characteristics are:

- Ambiental temperature: -20°C +65°C
- Aluminium outer tube and pushrod
- IP Grade: IP54
- Input voltage: 24 VDC
- External encoder: a feedbacking process of stroke
- Powder metallurgy gear
- Max load force: 900 N

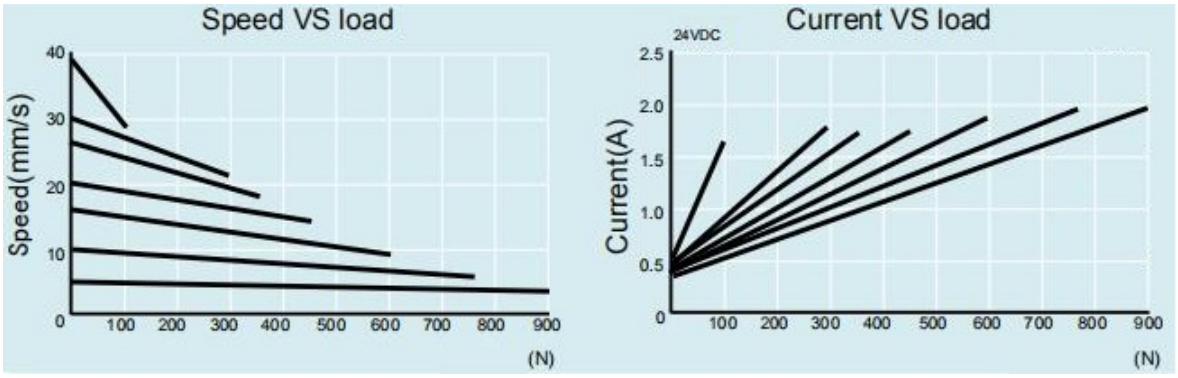

Figure 4.4: Performance diagrams.

- Duty cycle: 20%
- Max static load force: 2300 N
- Working life: 50 000 complete cycles
- Stroke 300 mm (±2 mm)
- Weight 1.11kg

4.1.2 H-Bridge

The rotation direction of the linear actuator's motors is controlled by using an H-bridge, where the direction of the current flow through the motor is reversed. For this purpose, the L298N (see Fig. 4.5) is a motor driver that controls the velocity and direction of the two linear actuator's DC motors.

The h-bridge can drive DC motors that with voltages between 5 and 35 V, with a peak current up to 2 A, due to the two linear actuator motors that work at 24 V with a peak current up to 1 A, the selection of this L298N driver is the best option.

The L298N driver applies signals from the microcontroller to make the motors rotate in a certain direction, and variate the duty cycle to control the velocity. To measure the velocity and position of the linear actuator is necessary a control system with feedback. An encoder in each DC motor triggers and updates the duty cycle of the motor. Eventually, this will result in the linear motor's rod reaching its target.

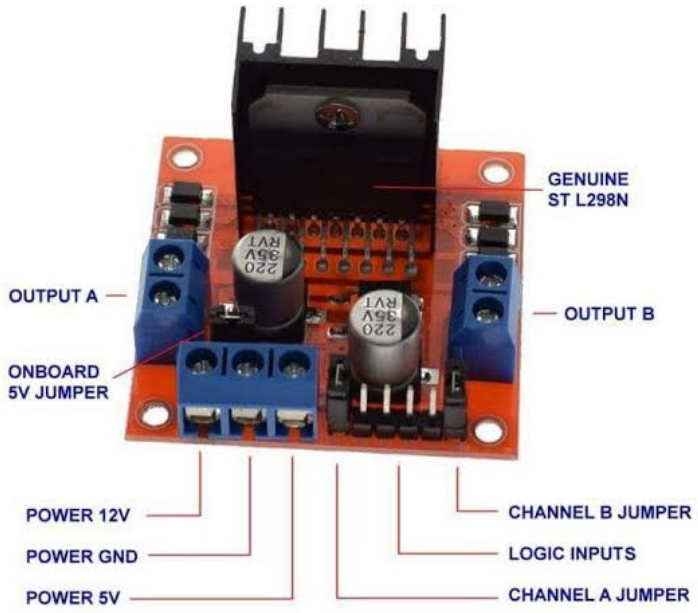

Figure 4.5: L298N Driver.

4.1.3 PWM DC Motor Control

Pulse width modulation (PWM) allows adjusting the value of the voltage (0 V to 24 V) that's going to the linear actuator motor by turning on and off the power at a fast rate. Since the speed depends on the pulse width when modifying the PWM the speed increases or decreases depending on the width. Some important parameters are:

- The ratio of amplitudes between the carrier signal and the modulator, it is recommended that the latter does not exceed the carrier's peak value and is centered on its average value.
- The frequency ratio, where it is generally recommended that the ratio between the carrier frequency and the signal frequency be 10 to 1.

4.1.4 Nucleo F767ZI

The proposed control is provided by the microcontroller Nucleo F767ZI controller to the controlled system. The controller board is connected by means of a wire, with the USB slot of the PC that allows for rapid control prototyping (RCP) and the output pines give the control signal, the implementation of RCP offered by Matlab/Simulink permits reduce the complexity in the programming of the board [77]. The Nucleo F767ZI can guarantee adequate sampling precision for the controllers designed for this project. It contains the low-level (general purpose input/output for sensors, actuators, adc, timers, etc.) and high-level (trajectory/tension controllers) control strategy.

4.1.5 Encoder

The LPD3806-400BM-G5-24C is a digital incremental encoder that has two outputs, A and B, which generate square pulses which are 90° out of phase, and this is the key design element that will provide the quadrature encoder its functionality. Its resolution is 400 pulses per revolution (PPR), with the use of the NUCLEO F767ZI is possible for the counter to count the rising and falling edges with both channels (A and B), resulting in a quadruple (x4) the number

of pulses (1600 PPR) with a resolution of 0.225. This kind of encoder has many advantages such as against humidity and dust, it is lightweight, small in size, low cost, able to resist a rotation speed of up to 5000 revolutions per minute as well as being fully compatible with most commercial microcontrollers such as Arduino, PIC, AVR, COP, DSP, STM32, etc.

4.1.6 Load cell

The implemented load cells are the JLBM-1-100, which have a capacity of 100 N with a sensitivity of 2.0 ± 0.1 mv/V, both cells are energized with a voltage of 9 V. The use of this project is to measure the tension of the springs, therefore these values serve by means of feedback and the corresponding control can be adjusted before the desired reference tension. The measure tensions are read from the 12-bit ADC on the Nucleo F767ZI board.

4.1.7 Control Algorithm

The type of control selected is PID, PD, Super-twisting, and asymptotic sliding mode control algorithms which operate by using feedback to match a setpoint or a reference using an external device, in this case, encoders and load cells that call an external function. This function or algorithm computes the selected control algorithm, by changing the DC motor's duty cycle.

The control algorithm made in Matlab & Simulink has tucked away in the function "control( )" with Rapid Control Prototyping in the SW4STM32. It is worth mentioning that the capabilities of generating Matlab & Simulink source code allows users to implement complex control algorithms without the need to write code. This allows the user to import the generated function into the SW4STM32 software to access and write a program that uses the advanced options of the microcontroller. The "control()" function characteristics are:

- Updates error position and tension
- Checks to see if the actuator's rod has reached its target (and if it has, stops the loop)
- Checks if the handle has reached the desired position
- Updates the output (duty cycle) of the control loop
- Control the duty cycle to the specified position and tension reference

4.2 Analysis on elastic elements

To make a stiffness adjustment in the device, it was necessary to perform the analysis of two elastic elements, Thera-Band® tubes, and springs, of which the following analysis was performed:

4.2.1 Thera-Band®

Since an alternative for assisted and active rehabilitation therapy is resisted-assisted and resisted exercises, the use of elastic resistance, such as elastic tubes and bands, with various levels of resistance can be used to do different exercises, their use is simple, are portable, can be used anywhere and low-cost materials. The consequences of movement with progressive elastic resistance have been investigated for some research as in [78] and the results demonstrate the effectiveness of using such a method in order to develop muscle and endurance.

The use of these elastic resistance tools seems intuitive like Thera-Band® elastic tubes are simple-to-use tools for multipurpose physical training with increasing strength. They provide

variable resistance and tension, the more the band or tubing is stretched, the greater the resistance. But its resistance is not characterized and its tension may vary depending on the elongation. Thera-Band® uses color progression resistance as can be seen in Fig. 4.6.

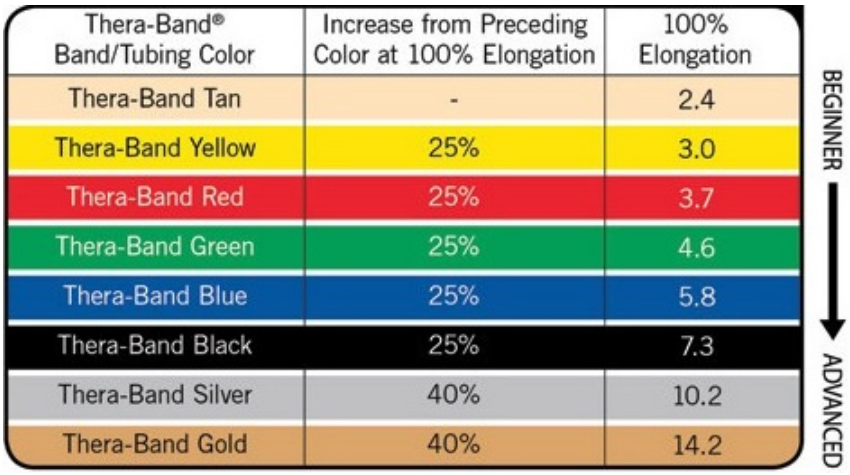

Figure 4.6: Thera-Band® color progression chart [7].

4.2.2 Characterizing the elastic tubing

Resistance training exercises using elastic tubing depend on the properties of polymers and thickness, which dictate the level of resistance and the amount of potential energy stored. The level of resistance changes according to the elongation of the material. The mechanical properties of tubing are often compared to the dynamics of springs in relation to stiffness but in the literature, there is no analysis of the Thera-Band tubing that is used in this thesis, for this reason, it is necessary to characterize it to determine if it is useful for the project.

A sample of 30 cm in length of Thera-Band® yellow tubing was taken, from which 10 stress tests were taken, the results obtained are shown in Table 4.1, and the graphic behavior is shown in Fig. 4.7.

Table 4.1: Tension generated for a percentage of Thera Band® yellow.

Deformation x (m)	% Elongation	Force (N) median
0.03	10	2.34
0.06	20	4.9
0.09	30	6.86
0.12	40	8.53
0.15	50	10.03
0.18	60	11.26
0.21	70	12.43
0.24	80	15.55
0.27	90	14.42
0.30	100	15.42
0.33	110	15.85
0.36	120	16.72
0.39	130	17.66

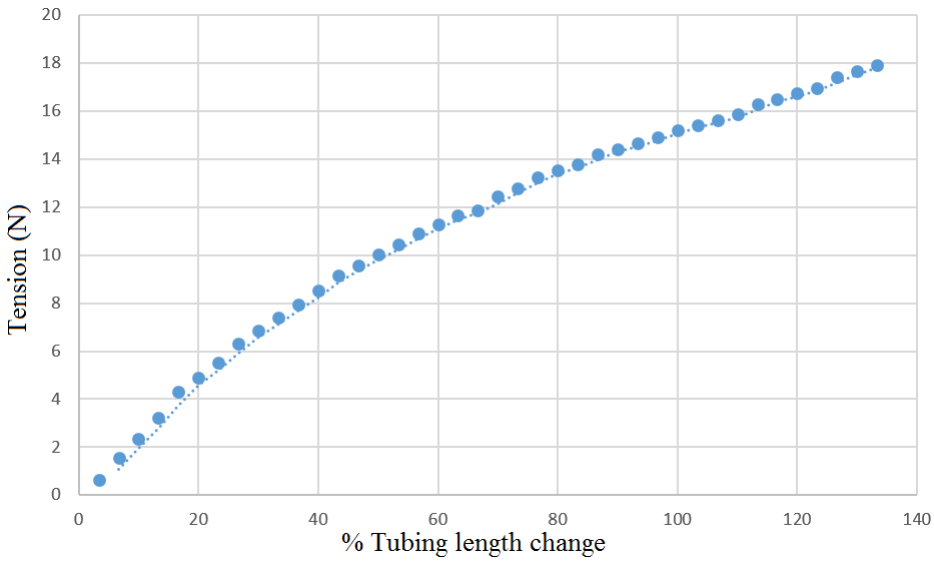

Figure 4.7: Tension generated for percentage change in length for Thera-Band® yellow color.

Linear regression was used to calculate the tubing tension equation, given by:

$$T = -92.405\delta_i^2 + 74.942\delta_i + 0.8163 \tag{4.1}$$

therefore, the stiffness constant k of the elastic cable varies as the cable is deformed. Giving us the next equation:

$$k = 355.92\delta_i^2 - 250.78\delta_i + 96.089 \tag{4.2}$$

Taking into account that the elastic cable is initially tensioned to a length of 44 cm and taking into consideration that its initial length is 30 cm, the length of the elastic cables is shown in Fig. 4.8 without the action of the linear actuator. The tension in the cables produced by the deformation is shown in Fig. 4.9.

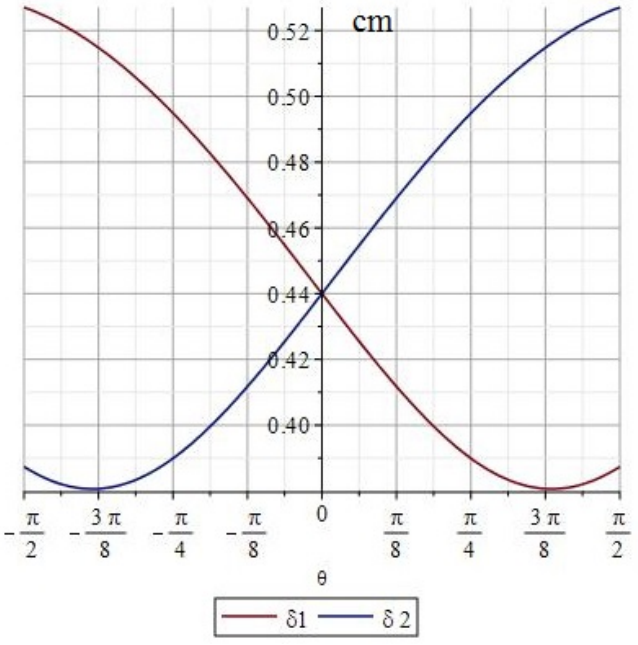

Figure 4.8: Elastic cable length.

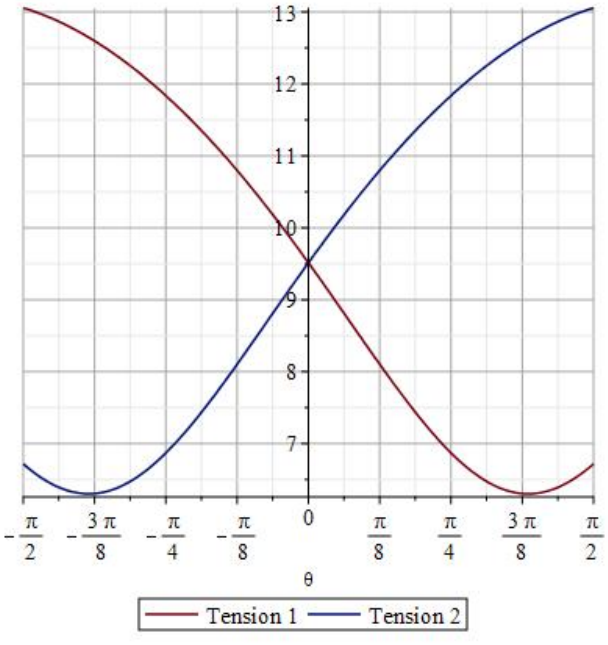

Figure 4.9: Elastic cable tension.

4.2.3 Springs

Given the linear characteristics of springs we introduce tension springs instead of elastic cables, from Lee Spring® and one more manufactured in a tool workshop, the chosen parts are:

- LE 034D 14 M
    * Outside diameter: 9.524 mm
    * Wire diameter: 0.863 mm
    * Maximum load: 20.460 N
    * Free length: 114.300 mm
    * Rate: 0.07 N/mm
    * Maximum length: 347.725 mm
    * Initial tension: 2.224 N
    * Material: Zinc plate and bake per ASTM B633
    * Number of coils: 113.3
- LE 031D 11 M
    * Outside diameter: 9.524 mm
    * Wire diameter: 0.787 mm
    * Maximum load: 15.123 N
    * Free length: 76.199 mm
    * Rate: 0.07 N/mm
    * Maximum length: 251.206 mm
    * Initial tension: 1.334 N
    * Material: Zinc plate and bake per ASTM B633
    * Number of coils: 75.6
- LE 026C 15 M
    * Outside diameter: 6.35 mm
    * Wire diameter: 0.66 mm
    * Maximum load: 13.788 N
    * Free length: 127 mm
    * Rate: 0.06 N/mm
    * Maximum length: 325.12 mm
    * Initial tension: 1.779 N
    * Material: Zinc plate and bake per ASTM B633
    * Number of coils: 176
- Manufactured
    * Outside diameter: 12.25 mm
    * Wire diameter: 1.36 mm

Table 4.2: Tension data for the percentage of change in length for springs.

Def. (cm)	Elong. (%)	034D14M Force (N)	Elong. (%)	031D11M Force (N)	Elong. (%)	026C15M Force (N)	Elong. (%)	Manufac. Force (N)
1	8.75	2.20	13.12	1.23	7.87	2.40	4.20	4.95
2	17.50	3.68	37.73	2.03	15.75	2.90	10.70	7.31
3	26.25	4.53	48.23	2.83	23.62	3.45	14.37	9.18
4	35.00	5.30	59.38	3.63	31.50	4.00	18.18	10.99
5	43.74	6.13	69.55	4.48	39.37	4.50	21.78	12.84
6	52.49	6.85	80.38	5.33	47.24	5.05	25.53	14.64
7	61.24	7.70	89.90	6.10	55.12	5.60	29.00	16.49
8	69.99	8.50	101.05	6.88	62.99	6.15	32.81	18.30
9	78.74	9.28	111.55	7.73	70.87	6.68	36.48	20.12
10	87.49	10.05	121.72	8.48	78.74	7.20	40.09	21.87
11	96.24	10.80	131.89	9.25	86.61	7.78	43.70	23.65
12	104.99	11.58	141.73	10.10	94.49	8.23	47.24	25.42
13	113.74	12.43	151.90	10.90	102.36	8.85	50.85	27.35
14	122.48	13.15	163.06	11.65	110.24	9.35	54.66	29.03
15	131.23	13.95	172.57	12.43	118.11	9.83	58.14	30.77
16	139.98	14.88	183.07	13.20	125.98	10.33	61.81	32.64
17	148.73	15.70	195.21	14.08	133.86	10.88	65.81	34.55
18	157.48	16.53	206.04	14.93	141.73	11.43	69.55	36.44
19	166.23	17.33	216.87	15.65	149.61	11.83	73.29	38.08
20	174.98	18.10	227.37	16.50	157.48	12.43	76.97	39.97

* Free length: 120 mm
* Initial tension: 5.46 N
* Number of coils: 64

Checking the spring stiffness constant, it was shown that it varies with respect to those provided by the supplier, in such a way that the spring stress tests obtained the following results in Table 4.2.

The spring linear behavior is shown in Fig. 4.10 where a linear regression was utilized to obtain the spring tension equation from the amount of elongation. Given the following tension equations:

- LE034D14M:

$$T = 79.701x + 2.10 \tag{4.3}$$

- LE031D11M:

$$T = 79.435x + 0.54 \tag{4.4}$$

- LE026C15M:

$$T = 53.018x + 1.86 \tag{4.5}$$

- Manufactured:

$$T = 181.77x + 5.46 \tag{4.6}$$

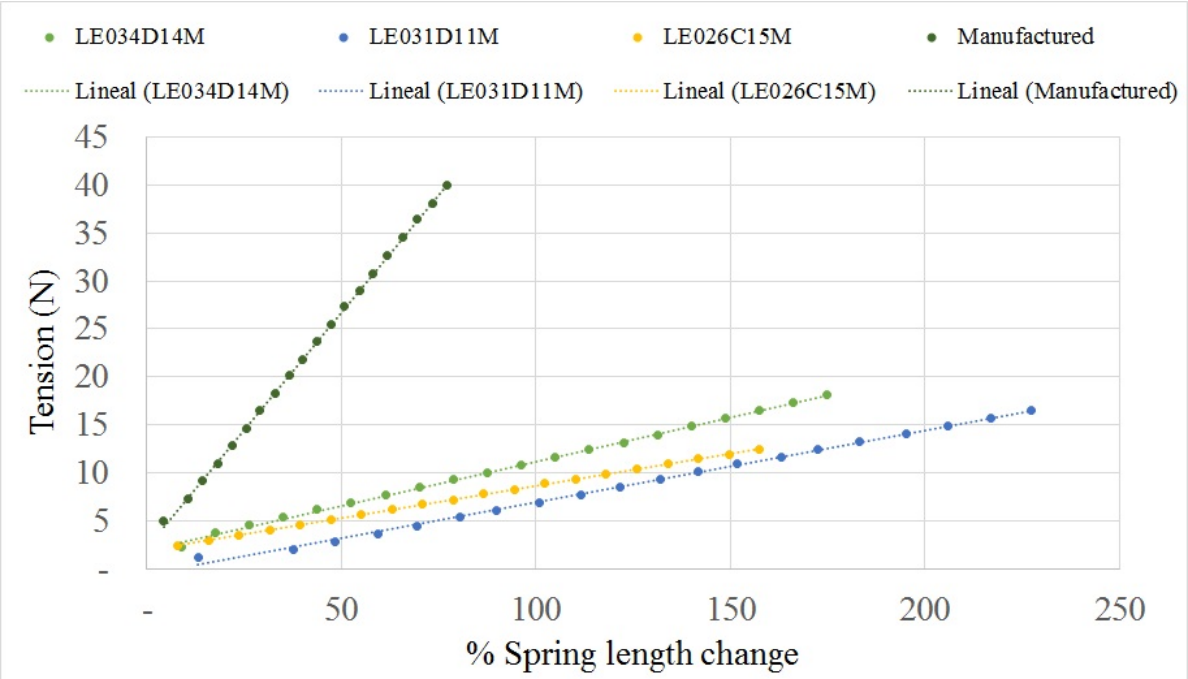

Figure 4.10: Tension generated for percentage change in length for Lee Spring® and a manufactured spring.

where x is the suffered elongation.

This information is useful in the selection and suitability of tubing or spring, as well as the reduction of operational costs in rehabilitation programs and training, since the tubing is about 1/10 part of the cost of spring but its behavior is non-linear and depends on the color and length of the tubing.

Spring damping

Even when behavior spring seems like expected, they present a damping constant. For example, for the LE034D14M several tests were carried out to determine the assumed constant. The free vibration trace measurement shows a 77.77% reduction in vibration after 8 cycles (see Fig. 4.11).

The damping ratio is a parameter denoted by ζ (zeta) that characterizes the frequency response of a second-order ordinary differential equation. For a mass-spring-damper system, where m is the mass, c the damping coefficient, and k spring's stiffness constant, the system's equation of motion is:

$$m\frac{d^2x}{dt^2} + c\frac{dx}{dt} + kx = 0 \tag{4.7}$$

the equation to the critical damping coefficient:

$$\zeta = \frac{c}{c_d} = \frac{actual \;\; damping}{critical \;\; damping} \tag{4.8}$$

the critical damping coefficient is given by:

$$c_d = 2\sqrt{k \cdot m} = 2m\sqrt{k/m} = 2m \cdot \omega_n \tag{4.9}$$

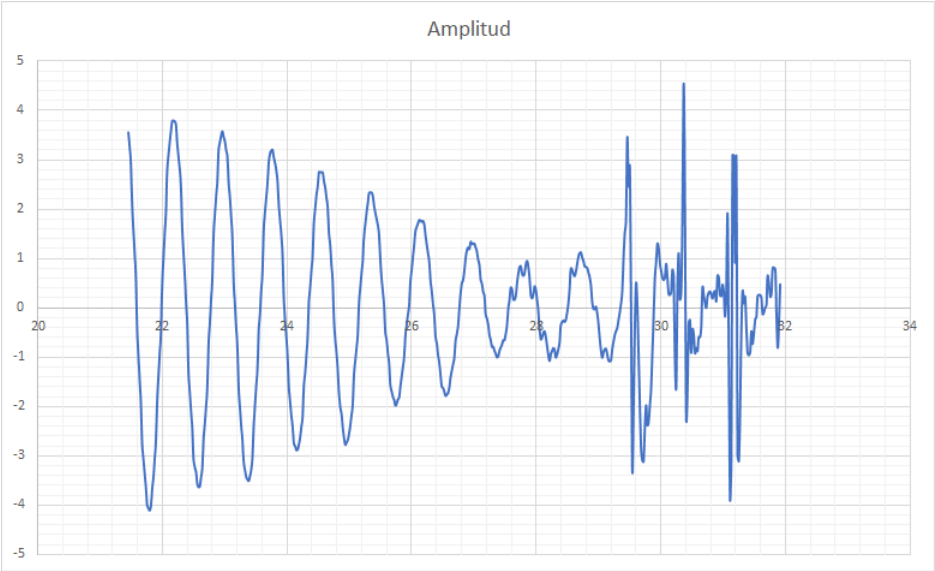

Figure 4.11: Vibration of spring with a mass of 1.125Kg.

where $\omega_n = \sqrt{k/m}$ is the natural frequency of the system.

The logarithmic decrement represents the rate at which the amplitude of a free-damped vibration decreases δ

$$\zeta = \frac{1}{\sqrt{1 + \left(\frac{2\pi}{\delta}\right)^2}} \tag{4.10}$$

where

$$\delta = \ln \frac{x_1}{x_2} \tag{4.11}$$

where x_1 and x_2 are the vibration amplitudes at two successive peaks of the decaying vibration.

The system consists of the following parameters:

- m=1.126kg
- k=79.701N/m

Performing the operations with the given equations we obtain

$$c = 0.5653 \quad \text{N·s/m} \tag{4.12}$$

which is the spring damping constant.

4.3 Load cells characterization

For the characterization of the two load cells, the instrumentation amplifier AD620AN and specific weights were used, the implemented circuit is shown in Fig. 4.12.

Each load cell was fed with a voltage of 9V, and the amplifier AD620AN was modified the excitation voltage from 3.3 V to 5 V obtaining better results with 5 V. The differents weights

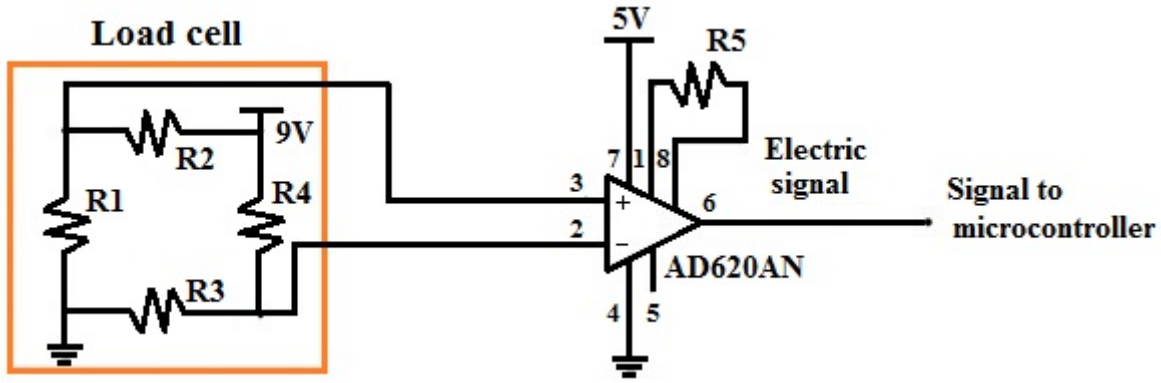

Figure 4.12: Load cell circuit.

Table 4.3: Load cells.

Load cell 1		Load cell 2	
ADC	T(N)	ADC	T(N)
4095	0	4095	0
4070	5.9	4090	6
4030	10.8	4070	10
3950	16	4025	20
3810	26	3970	25
3730	31.1	3900	30
3560	41	3800	40
3430	51.2	3580	51.5
3330	56.4	3300	65.4

were measured with a digital force gauge. The AD620AN output signal is connected to an ADC of the NUCLEO STM32F767ZI, obtaining the Table 4.3:

From the values of the Table 4.3, it is obtained a function that represents the tension getting the following equations:

$$T_1 = 0.00003652045 + 0.04576167A_{dc} + 6.341392 \times 10^{-7}A_{dc}^2 - 2.8408859 \times 10^{-9}A_{dc}^3$$
$$T_2 = 6.2859166 \times 10^{-6} + 0.007550844A_{dc} + 0.0000195626A_{dc}^2 - 5.125059047 \times 10^{-9}A_{dc}^3$$

Where T is the tension in Newton and A_{dc} the values of the ADC. Regarding Table 4.3, higher values were not obtained since the project does not contemplate forces greater than 60N.

To verify the effectiveness of the function, a graph with three different weights was obtained (see Fig. 4.13a), which were 41 N, 51.2 N, and 56.4 N. These were measured by the load cell in such a way that they hung, once the measurement was made it was removed and then another weight was put on it. It should be noted that in Figure 4.13b, the noise is evident, which is why a digital filter was made for each load cell in MATLAB & Simulink using RCP [77], the resultant digital filter function is integrated into the main code in SW4STM32. Obtaining the following results showed in Figure 4.13:

4.4 Model fabrication

Because the physical model is an innovative design, many of the pieces to perform the mentioned tasks are designed. For this reason, some pieces are manufactured using three-dimensional (3D)

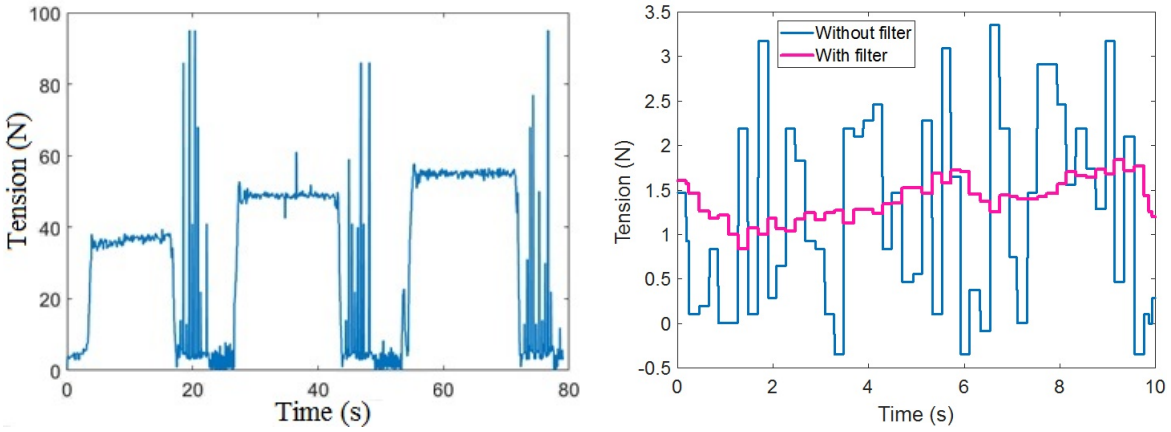

(a) Three different weights.

(b) With filter and without digital filter.

Figure 4.13: Tension measurement.

printing, although others will be purchased if they exist under the requirements. The factors considered for the material selection include:

- Cost of the material
- Its ability to manufacture
- Mechanical attributes
- Tensile strength
- Yield strength

The use of Polylactic Acid (PLA) is the best choice for manufactured pieces because of its properties in strength and stiffness than both Acrylonitrile Butadiene Styrene (ABS) and nylon. With a low-cost of PLA is one of the easiest materials to 3D print successfully.

Throughout the construction of the physical model, some tests were carried out on the parts design and the function they fulfilled. Such is the case of Fig. 4.14 where these parts were replaced by other pieces. Figure 4.14a shows the handle, in which the cables were attached to it by the four holes that are observed, it was changed because a pulley in the handle makes the torques perpendicular to it. A motor coupling was designed for the encoder (see Fig. 4.14b), but there was significant wear, which had to be changed for a metal one. Figure 4.14c shows the handle pulley in the system, which was changed to increase the angular velocity. The current handle and handle pulley designs are shown in Fig. 4.15.

Figure 4.16 shows other parts that were printed: where Fig. 4.16a shows the piece that joins the encoder with the linear actuator, Fig. 4.16b is a 90° joint for the aluminum profiles of the structure, two pieces serve as a spring-load cell-rod union of the actuator (Fig. 4.16c) and Fig. 4.16d is one of the pulleys that serve to redirect the cables inside the structure.

(a) Handle.

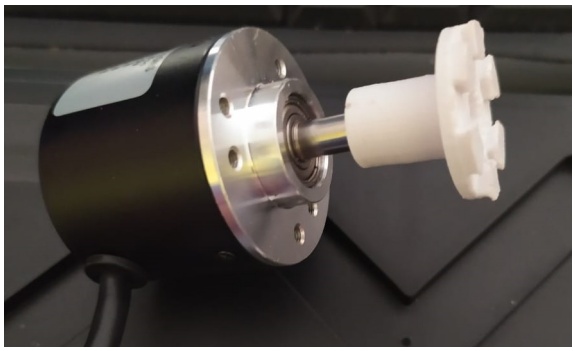

(b) Encoder union.

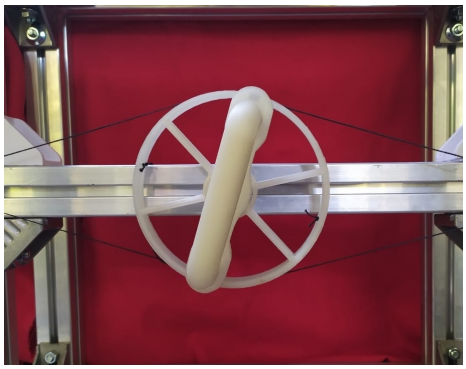

(c) Handle pulley.

Figure 4.14: Replaced parts.

(a) Handle.

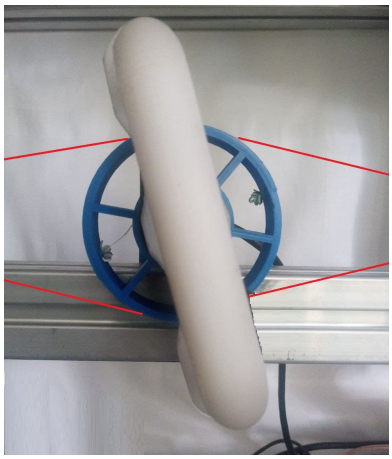

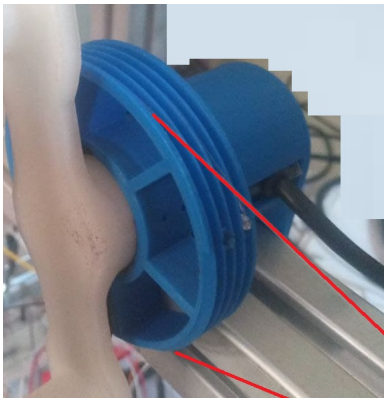

(b) Handle pulley.

Figure 4.15: Handle and handle pulley.

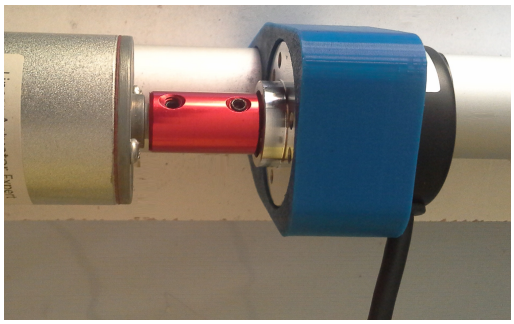

(a) Encoder union.

(b) 90 degree union.

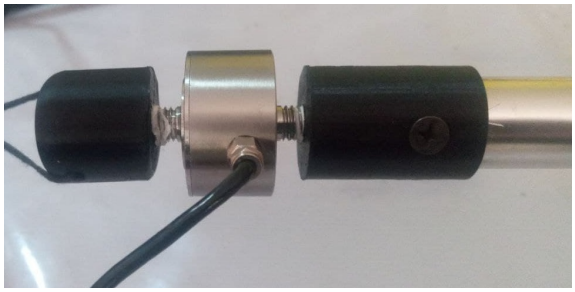

(c) Load cell union.

(d) Pulley.

Figure 4.16: Other manufactured parts.

Chapter 5

Adjustable stiffness rehabilitation device

The rehabilitation system reported in this paper includes four non-elastic cables driven by two electrical linear actuators, a guiding mechanism consisting of a series of pulleys that serve to redirect the cables, two springs, two load cells, and a handle with a pulley that reproduces angular displacements to perform wrist-forearm supination-pronation rehabilitation protocols (see Fig. 5.1).

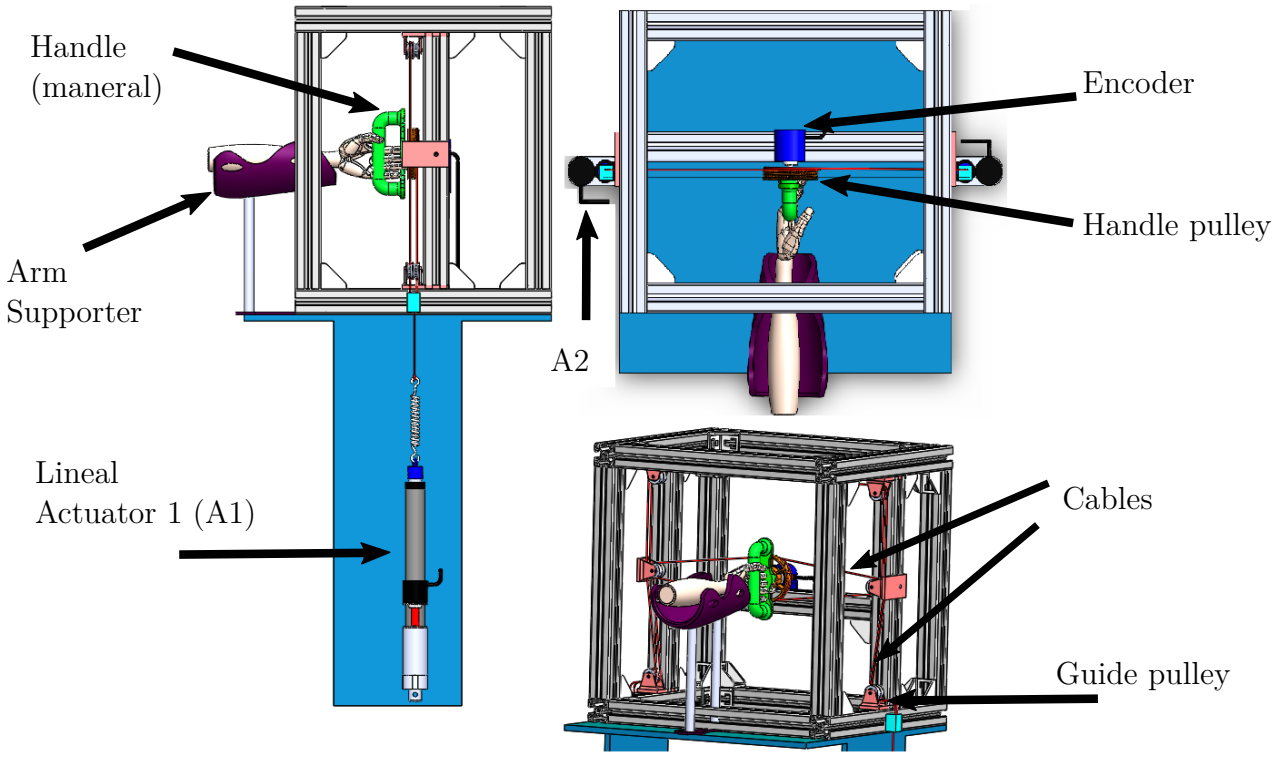

Figure 5.1: Mechanical structure.

The rehabilitation structure should accomplish the next goals:

- The size of the adjustable stiffness device should be adjusted to suit different patient sizes.
- The rehabilitation structure should coordinate wrist and forearm movements.
- The movements of the structure should be smooth, while the axes of rotation should support the rotations of the limbs of the human body, from which they should protect the patient from any injury.

5.1 Mechanism description

With the purpose to obtain optimal supination-pronation rehabilitation, an adjustable stiffness device, it is designed in such a way that when changing its shape, the device can measure and modify the tensions which it is subjected. The proposed tensegrity system is composed of two springs, four cables, two linear motors, three encoders, two load cells, and a microcontroller, the purpose of the structure is to rehabilitate the wrist-forearm through the movement of pronation and supination that covers a range of motion in the plane from -90° to 90°.

The springs have the objective of generating a variable tension that will be controlled by the linear motors, while the cables will transmit the movement of the motors to the springs and the handle. Figure 5.2 illustrates the way the cables are connected to each linear actuator through a spring, a load cell and two connectors (in blue).

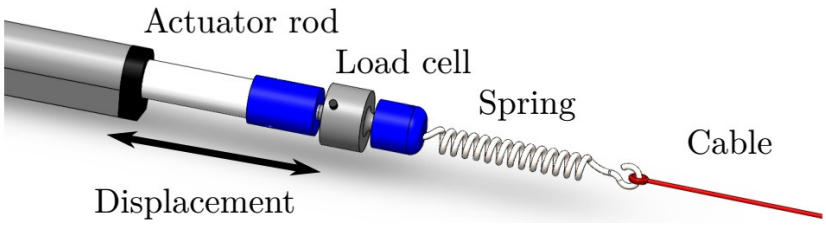

Figure 5.2: Linear actuator, load cell, spring and cable assembling.

Each spring is attached to two rigid cables, and the four cables are attached to the handle (see Fig. 5.1), where it will act in the plane (x, y), but it will only make a change of rotation θ this in order to analyze the change of the configuration, a change in the potential energy of the system and therefore the tensions in the elastic cables.

The system will allow greater flexibility in the forces and movements of the therapy such that the designed application helps patients to overcome muscular weakness. When a passive movement is performed, the device is in charge of performing the movements without any intervention (strength) of the patient. On the other hand, when an assisted-resisted movement is performed the elastic cables will play an important role to create greater tension and with this to create muscle strength in the human member.

In accordance with traditional rehabilitation protocols for the wrist-forearm (see [5,47,48]), the following procedure was designed to be used in the rehabilitator device:

- The hand of the affected limb of the patient will grasp the handle either sitting or standing, if the patient had any discomfort the forearm would be accommodated in a supporter.
- The supination-pronation movement is performed with the arm fully extended or with the elbow at 90°.
- The supination-pronation ROM that the patient performs will be based on the evaluation previously made by a physical therapist.
- The variation of the tension in the rehabilitative device will be according to how the patient is evolving.

To achieve correct wrist-forearm rehabilitation, the rehabilitation device is capable of performing the three rehabilitation stages according to the ROM of each patient since not everyone can perform a ROM of -90° to 90°, the exercises, and their resistance level will be previously established by a physical therapist. The rehabilitator performs the three stages as shown in [8].

Figure 5.3 depicts the movements of the wrist-forearm with the handle, four forces are present f_1, f_2, f_3, and f_4 that produce the torque τ. The two movements supination (see Fig. 5.3a) and pronation (see Fig. 5.3c) that the rehabilitator, the two of then start from the neutral position (see Fig. 5.3b).

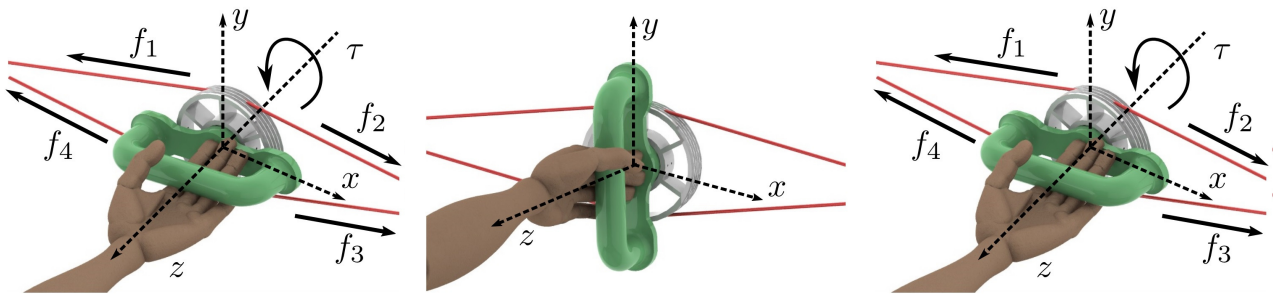

(a) Supination (b) Neutral position (c) Pronation

Figure 5.3: (a)Supination, (b) Neutral position, (c) Pronation [8].

5.2 Modeling

Figure 5.4 represents the one degree of freedom (DOF) system aimed at reproducing the angular movements shown in Fig. 5.3.

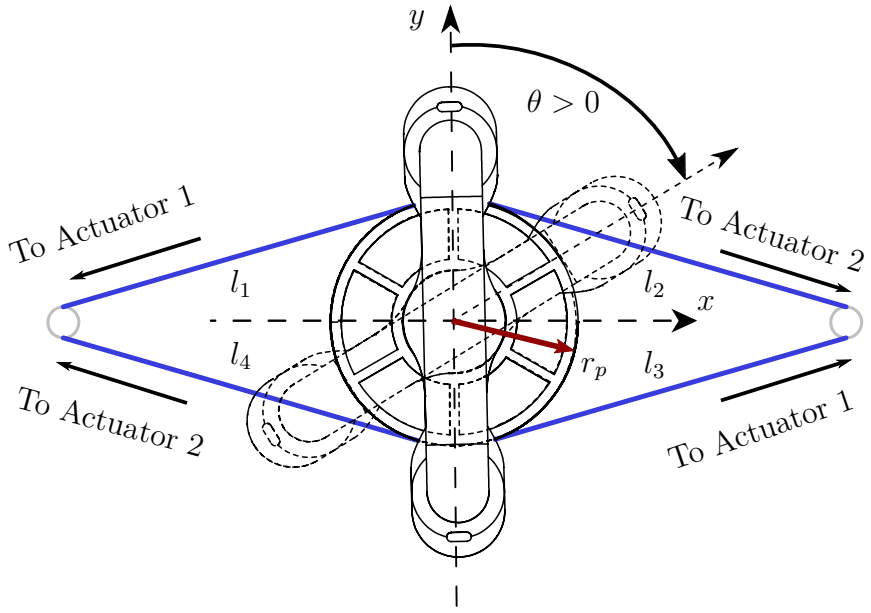

Figure 5.4: Handle with pulley and cables.

5.2.1 Abbreviation

The main parameters of the system are:

- u_i are control inputs.
- l_i are the initial lengths of spring.

- l_0 is the free length of the spring.
- θ is angular motion of the handle.
- r_p is the pulley's radius.
- δ_i is the elongation or shortening of the spring.

The dynamic model is developed using the Euler-Lagrange equations that constitute an alternative formulation to the classic Newtonian formulation. The justification for using them is that it leads to the correct equations of motion, with the following assumptions.

5.2.2 Conditions

The initial configuration of the system.

- The initial configuration is in a *prestressed* state. Such that the deformation suffered is:

$$\delta_i = l_i - l_0 \tag{5.1}$$

- There is a geometric symmetry in each cable $l_1,\ l_2,\ l_3,\ l_4$.
- The mass of the springs and rigid cables are negligible.
- The mass of the handle with the approximate mass of the hand are the only ones considered.
- The stiffness constants of each springs are equal $k_1 = k_2 = K$.
- The free length of each elastic element is: $l_0 = l_{01} = l_{02}$.
- The initial length is constant and equal in each spring.
- The rotation movement is considered without friction.
- The assigned material and dimension to each element of the structure is defined by the designer.
- Tension are delimited by:

$$T_{min} \leq T_i(\theta, \dot{\theta}) \leq T_{max} \tag{5.2}$$

θ is generated by the combined action of four forces f_1, f_2, f_3 and f_4 acting through cables l_1, l_2, l_3 and l_4, these cables are tangent to r_p. The motion of the rehabilitator device is executed on the xy plane. Then, the angular motion's torque τ generated is parallel to the z axis. In Fig. 5.4, the handle initially is at the neutral position $\theta = 0$. If the handle rotates clockwise, $\theta > 0$, otherwise $\theta < 0$ (if this initially is at the neutral position). There is a friction torque k_τ present in the relative angular displacements between elements (bearings and shafts, for instance) that is not considered.

Since cables are tangent to the handle, the couple of forces f_1-f_3 generate with respect to the point 0 the torque $\tau_{13} = 2f_{13}r_p$, while the couple f_2-f_4 generates the torque $\tau_{24} = 2f_{24}r_p$.

From the conditions, the elongations produced by the deformation of $\delta_1 = \delta_3 = \delta_{13}$ and the elongations produced by the deformation of $\delta_2 = \delta_4 = \delta_{24}$, the forces are calculated as:

$$f_{13} = K(l_i - l_0 + \delta_{13} + u_{13}) \tag{5.3}$$
$$f_{24} = K(l_i - l_0 + \delta_{24} + u_{24}) \tag{5.4}$$

where u_{13}, u_{24} are the input control displacements due to linear actuators. Then the total torque τ is written as:

$$\begin{aligned} \tau &= f_{13} + f_{24} = [2f_{13}r_p - 2f_{24}r_p] \\ &= 2r_pK(f_{13} - f_{24}) \\ &= 2r_pK[(l_i - l_0 + \delta_{13} + u_{13}) \\ &\quad -(l_i - l_0 + \delta_{24} + u_{24})] \\ &= 2r_pK[\delta_{13} - \delta_{24} + u_{13} - u_{24}] \end{aligned} \tag{5.5}$$

The handle experiences angular motion, then the kinetic energy E_k of the system is calculated by the Eq. 5.6

$$E_k = \frac{1}{2}I_{zz}\dot{\theta}^2 \tag{5.6}$$

where I_{zz} is the inertia moment of the system with respect to the z axis and $\dot{\theta} = \frac{d\theta}{dt}$.

Because there is no gravitational potential energy (E_{pg}) associated with the system, Lagrange's equation of motion is obtained by:

$$\frac{d}{dt}\frac{\partial \mathcal{L}}{\partial \dot{\theta}} - \frac{\partial \mathcal{L}}{\partial \theta} = F_i \tag{5.7}$$

where $\mathcal{L} = E_k - E_{pg}$ and F_i is the generalized external forces.

Therefore:

$$\mathcal{L} = \frac{1}{2}I_{zz}\dot{\theta}^2 \tag{5.8}$$

using Eq. 5.8 and defining the incremental deformation as $\Delta\delta_{14} = \delta_{13} - \delta_{24}$ and $\Delta u_{13} - \Delta_{24}$, it can be established that:

$$I_{zz}\ddot{\theta} = 2r_pK(\Delta\delta_{14} + \Delta u_{14}) \tag{5.9}$$

For θ to achieve its full movement, the next inequalities must be satisfied.
For $\theta < 0$:

$$\delta_{13} > 0, u_{13} > 0 \quad \text{and} \quad \delta_{24} < 0, u_{24} > 0 \tag{5.10}$$

For $\theta > 0$:

$$\delta_{13} < 0, u_{13} < 0 \quad \text{and} \quad \delta_{24} > 0, u_{24} > 0 \tag{5.11}$$

Where the displacement of δ_{13} and δ_{24} are:

$$\delta_{13} = -2\pi r_p\theta/360 \tag{5.12}$$
$$\delta_{24} = 2\pi r_p\theta/360 \tag{5.13}$$
$$\Delta_{14} = -\frac{4r_p\pi\theta}{360} \tag{5.14}$$

Thus Eq. 5.9 becomes 5.15

$$I_{zz}\ddot{\theta} = -\frac{8r_p^2 K\pi\,\theta}{360} + 2r_p K\Delta_{14} \tag{5.15}$$

Equation 5.15 relates the angle trajectories to measured angular displacement. Constants are defined:

$$\begin{aligned} c_1 &= -\frac{8r_p^2\pi K}{360 I_{zz}} \\ c_2 &= -\frac{c_f}{I_{zz}} \\ c_3 &= \frac{2r_p K}{I_{zz}} \\ \Delta u &= u_{13} - u_{24} \end{aligned}$$

Thus the second-order differential equation of the rehabilitation system with friction is:

$$\ddot{\theta} = c_1\theta + c_2\dot{\theta} + c_3\Delta u \tag{5.16}$$

with u_{13} and u_{24} as inputs of the linear actuator 1 and 2, respectively, which are connected to the cables l_1, l_3 and l_2, l_4. K correspond to the spring stiffness coefficient [N/m], r_p is the radius of the handle pulley [m], c_f is the viscous friction coefficient [kg·m^2/s], I_{zz} is the moment of inertia's handle [kg·m^2].

Equation (5.16) be written as in equation (5.17) representing a continuous linear system:

$$a\ddot{\theta} + b\theta + c\theta = \Delta u \tag{5.17}$$

where the following relations have been used: $a = 1/c_3$, $b = -c_2/c_3$ and $c = -c_1/c_3$. Then, by applying Laplace transformation to Eq. (5.17) and stablishing θ as the output of the system, the transfer function of the adjustable stiffness device is provided in Eq. (5.18).

$$G(s) = \frac{1}{a\,s^2 + b\,s + c} \tag{5.18}$$

5.2.3 Moment of inertia's handle

To calculate I_{zz} we took an approximation of the handle designed in SolidWorks (Fig. 5.5), where the detailed description of the I_{zz} with the measurements of the Hand Gripper are:

$$\begin{aligned} I_{zz} &= I_{zz1} + I_{zz2} + I_{zz3} \\ I_{zz1} &= \frac{M_1 R_1^2}{2} - \frac{M_2 R_2^2}{2} \\ I_{zz2} &= \frac{1}{12}M_3(a^2+b^2) + 4M_3\left(\frac{R_3^2}{2} + d_1^2\right) - 4M_5\left(\frac{R_4^2}{2} + d_1^2\right) \\ I_{zz3} &= 2M_6\left(\frac{R_5^2}{2} + d_2^2\right) + \frac{M_7 L^2}{12} \end{aligned}$$

the masses are $M_1 = 51.46g, M_2 = 2.97g, M_3 = 72.3g, M_4 = 11.5g, M_5 = 2.97g, M_6 = 10.18g, M_7 = 42.49g$

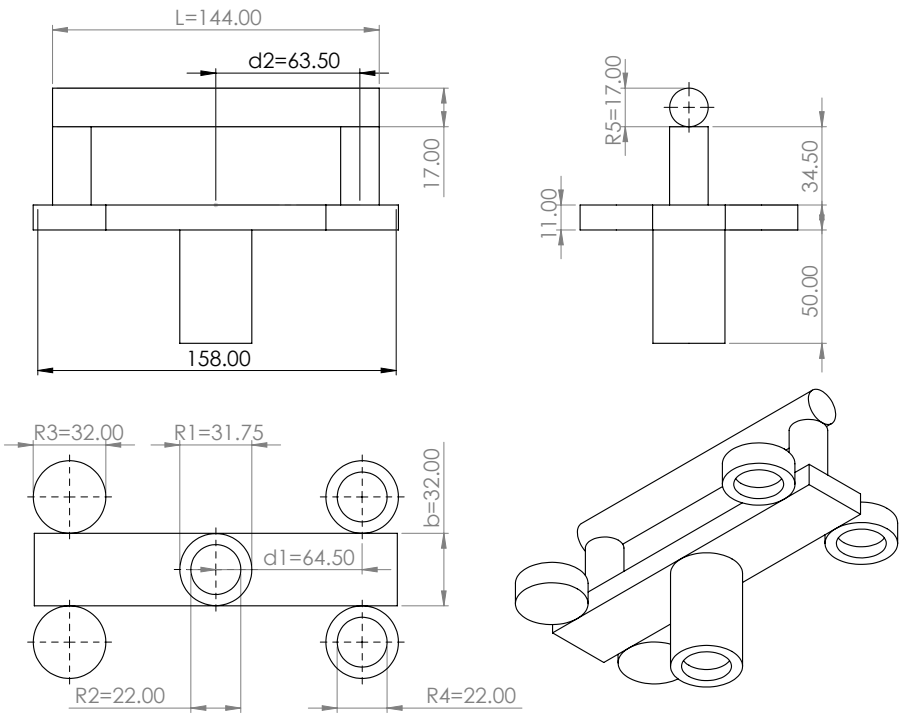

Figure 5.5: Measurements of the approximate handle.

Therefore the resulting I_{zz} is:

$$I_{zz} = 464061.98\text{g} \cdot \text{mm}^2 = 4.6406198 \times 10^{-4}\text{kg} \cdot \text{m}^2 \tag{5.19}$$

The handle designed in SolidWorks and fabricated with PLA has the following mass and moment of inertia (provided by mass properties SolidWorks):

- Mass= 209.37 grams
- I_{zz} =460987.98 gr·mm^2=4.6098798×10^{-4}kg·m^2

5.3 System behavior

With the defined workspace and the dynamic model developed, the configuration of the system in motion depends directly on its dynamic behavior and the proposed strategy aims to follow a defined path in the workspace of the actuator being controlled by the forces of this.

Now it is presented in two cases of deformation, a spring is taken and stretched 14 cm so that the system is pre-stressed, in the first case, there will be no displacements u_i made by the linear motors. In the second case, the deformation will occur when the linear motors have a displacement of 9 cm to 18 cm.

5.3.1 Case 1

Figure 5.6 shows the case that the inputs $u_1 = 0$ and $u_2 = 0$ and the springs are deformed due to the rotational movement of the handle. The red line shows the behavior of the spring connected to the cables l_1 and l_3 and the blue one the spring connected to the cables l_2 and l_4. The graph shows when the handle moves $\theta > 0$ the spring connected with the cables l_1, l_3 will be lengthened from 14 cm to 22.5 cm, while the springs in l_2, l_4 will be shortened from 14 cm to 8 cm when $\theta < 0$ the opposite happens.

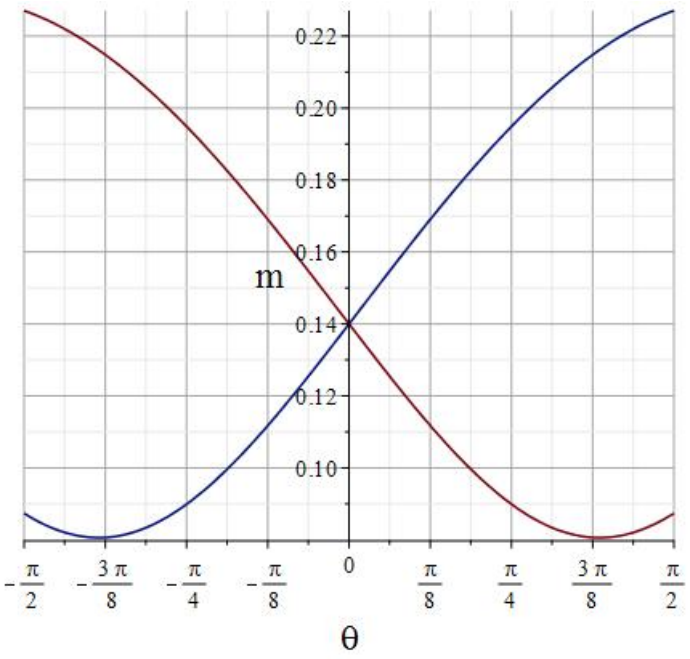

Figure 5.6: Spring length.

5.3.2 Case 2

Now the inputs u_1 and u_2 under the action of the linear motors will move in a range from 90 mm to 180 mm. The length of spring 1 is shown in Fig. 5.7 and the length of cable 2 is shown in Fig. 5.8. These figures show the behaviors of the springs through the actuation of the linear motors. Starting from $\theta = 0$ and an initial length of 14 cm, the spring will elongate from 22.5 cm to 32 cm when $\theta > 0$ and the linear motor that is connected to them contracts its stem (S1, S2) from 135 mm to 90 mm. On the contrary, it will be shortened from 14 cm to 8 cm if the stem that guides it makes a forward movement from 135 mm to 180 mm.

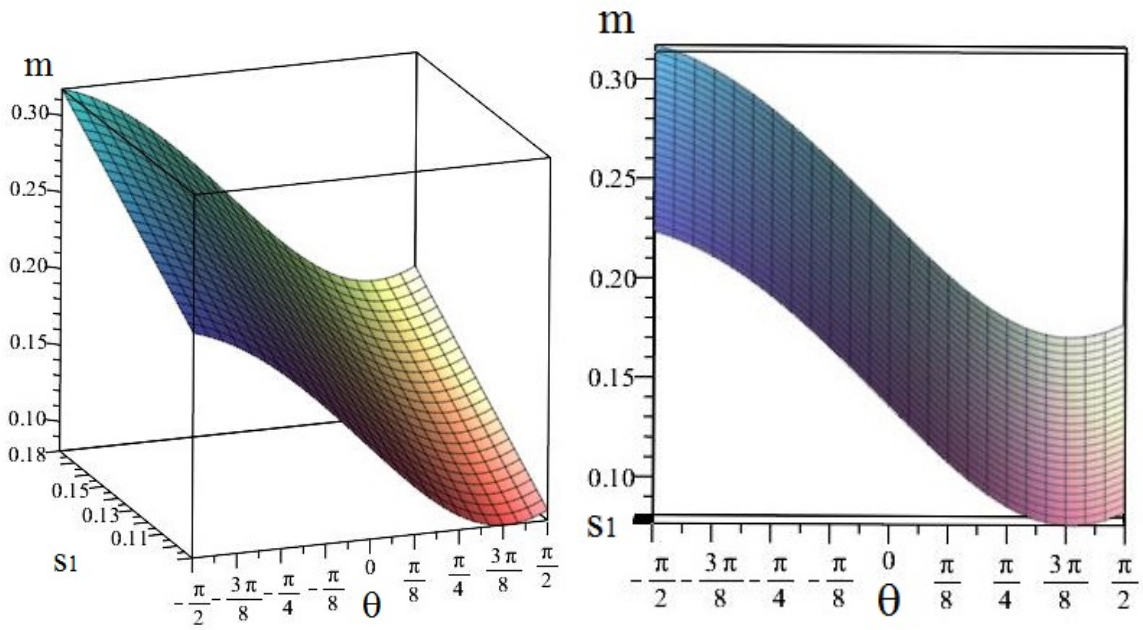

Figure 5.7: Spring 1 length with linear motor action.

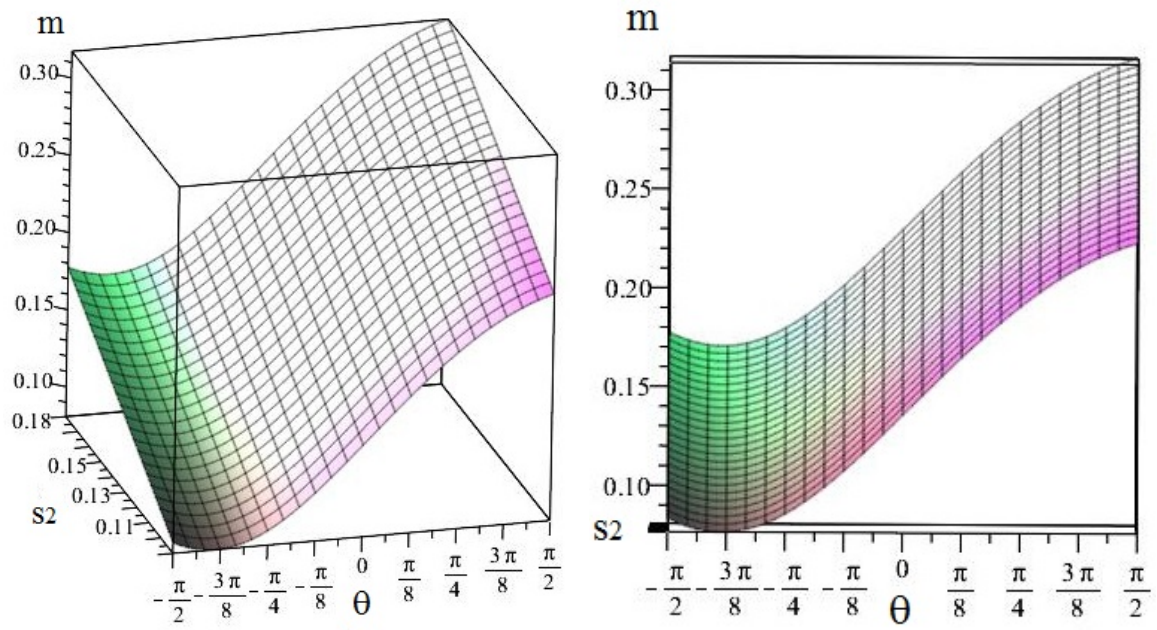

Figure 5.8: Spring 2 length with linear motor action.

5.3.3 Control actions

To design adequate control, it must be taken into account that there is no control theory in the design of this type of system. One consideration is that actions of local control can be distributed throughout the structure. Where the variation of the initial configuration will be made with the systematic variation of a member (Linear actuator) in which it will change position, the predefined solutions with maximum and minimum values in the coordinates will be estimated. It has to consider material, and structural failures, as well as propose a range of energy and restrictions of the elements involved. For control issues will not consider:

- Complex oscillatory movements
- Non-linear elastic interactions.

The control must modify the position and tension of the adjustable stiffness device. The control will be carried out by means of the linear motors, it is evident for the geometrical symmetry only 2 linear motors can be used u_1, u_2 which are linked to the deformation of the springs δ_1, δ_2 respectively.

5.3.4 Stiffness

The stiffness is the resistance of the 1-DOF stiffness variable rehabilitator to displacements when an external force F is applied. When $F = 0$, there are no external forces that modify the position of the system, that is the system is in equilibrium o in its initial position. The equilibrium system is when its potential energy is at a minimum, as shown in Fig. 5.9.

By differentiating the potential energy with respect to θ, it can get obtain the behavior of the force F expressed in the equation 5.20

$$F = \frac{\partial E_p}{\partial \theta} \tag{5.20}$$

The graph of 5.20 versus θ is comprehended as the stiffness profile (shown in Fig. 5.10).

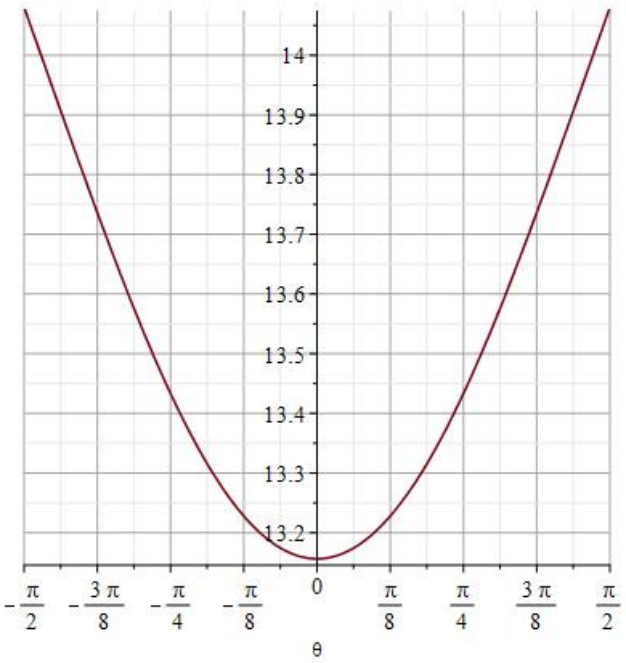

Figure 5.9: System potential energy.

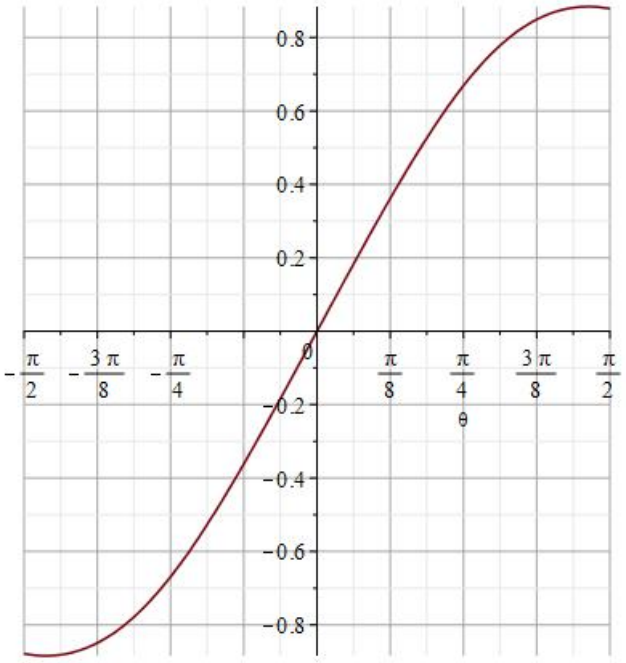

Figure 5.10: Stiffness profile.

The system stiffness K can be obtained with the partial derivative of equation (5.20) with respective to θ:

$$K = \frac{\partial F}{\partial \theta} \tag{5.21}$$

From Fig.5.11 it can be seen that when a tensile force is applied the stiffness increases, while it decreases when a compression force is used. The stiffness is related to θ and the critical value defined as θ_{min} that corresponds to a F_{min} from Figure 5.10. It is seen that the stiffness is at a local maximum when the system is in stable equilibrium while it is a local minimum when the system is in unstable equilibrium.

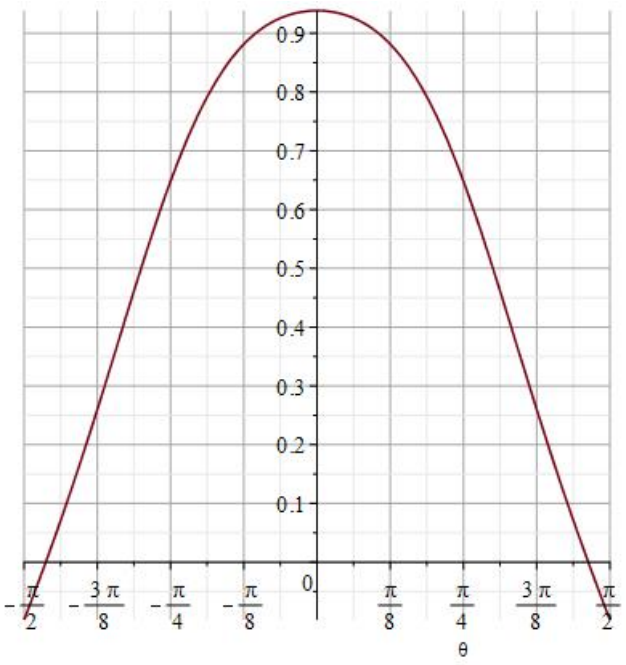

Figure 5.11: Stiffness.

The phase portrait of the system is shown in Fig. 5.12. Therefore the trajectories close to the equilibrium point can be guaranteed to stay within a cycle centered at the equilibrium point.

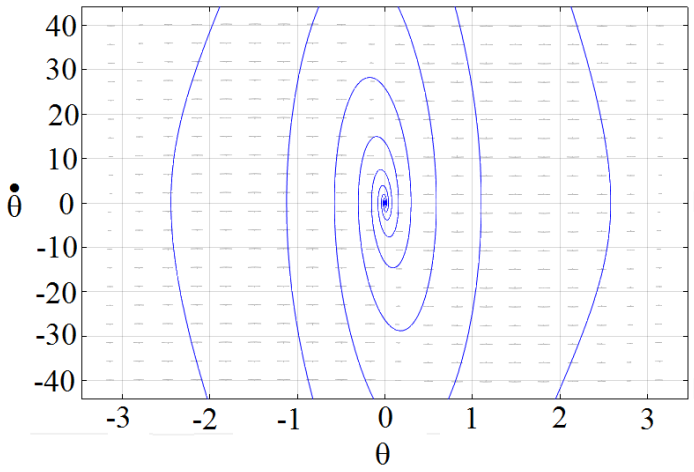

Figure 5.12: Phase portrait.

The steady-state response at 60° of the systems is shown in Fig. 5.13, which produces a change in the potential energy of the system (Figure 5.14).

The steady-state response at 45° of the systems is shown in Fig. 5.15, which produces a change in the potential energy of the system (Figure 5.16).

5.4 PID design controller

The PID controller is widely used in industrial processes and in general in any automatic process because is an accurate, stable, and reliable controller. This controller has the transfer function:

$$G_{PID} = K_p + \frac{K_i}{s} + Kd\,s \tag{5.22}$$

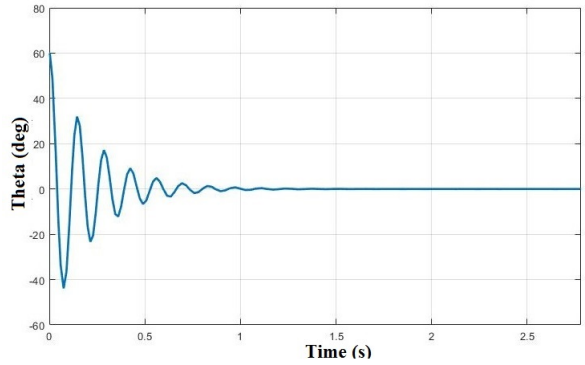

Figure 5.13: Steady-State Response at 60°.

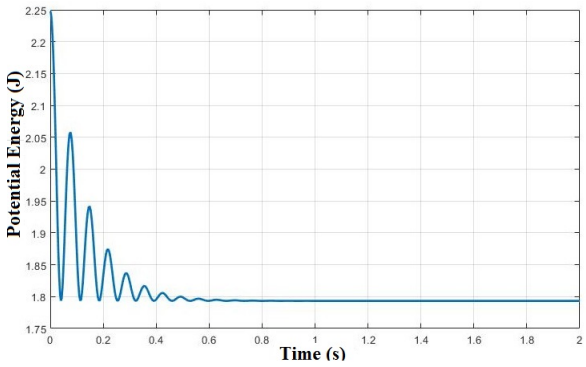

Figure 5.14: Potential energy at 60°.

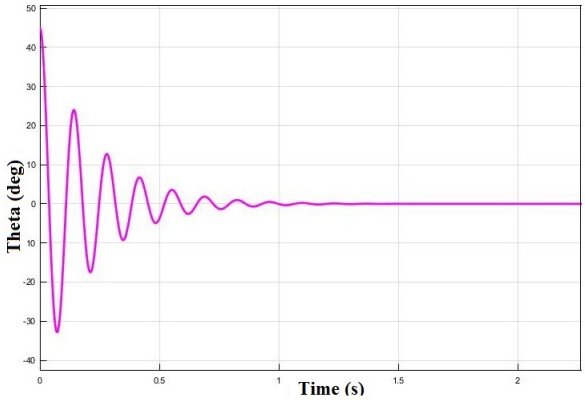

Figure 5.15: Steady-State Response at 45°.

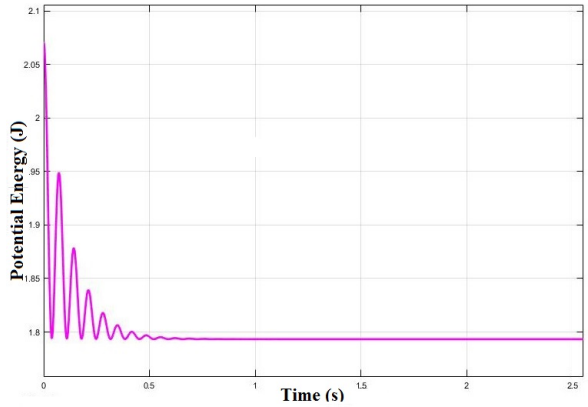

Figure 5.16: Potential energy at 45°.

The control law in the time domain is given by:

$$u = K_p\, e(t) + K_i \int_0^t e(\tau)d\tau + K_d \frac{de(t)}{dt} \tag{5.23}$$

The main purpose of using the control law (5.23) is to drive the error (e) to zero in a control loop feedback device.

From Eq. (5.18) and using the PID controller transfer function (5.23), the closed loop (G_{CL}) transfer function, with negative and unitary feedback, is given by:

$$G_{CL}(s) = \frac{K_d\, s^2 + K_p\, s + K_i}{a\, s^3 + (b + K_d)s^2 + (c + K_p)s + K_i} \tag{5.24}$$

The closed loop characteristic polynomial P_{CL} is provided in Eq. (5.25).

$$P_{CL}(s) = a\, s^3 + (b + K_d)s^2 + (c + K_p)s + K_i \tag{5.25}$$

Where K_p is the proportional gain, K_i is the integral gain, and K_d is the derivative gain of the PID controller.

To determine the ranges of the PID gains that will result in a stable system, the Routh-Hurwitz criterion is used. t is simple to verify that inequalities (5.26) need to be, simultaneously, satisfied in order to guarantee closed-loop stability of the system.

$$\begin{aligned} K_p &> 0 \\ K_i &> 0 \\ K_d &> 0 \\ (b + K_d)(c + K_p) &> a\, K_i \end{aligned} \tag{5.26}$$

Based on parameters values, $a > 0$, $b > 0$, $c > 0$ and $c > b > a$.

5.5 Asymptotic sliding mode controller (ASMC)

The SMC has been used in many applications, proving to be an efficient control technique, first-order SMC has high-frequency switching causing chattering which is an undesirable phenomenon in practical applications, the ASMC uses the sliding mode function in terms of control function derivative, becoming the controller algorithm into a continuous control [37]. Although the ASMC algorithm performs well in simulation, tracking error dynamics do not converge to zero in practical implementations, to overcome this difficulty in [79] an integral term of measurement error is added to the ASMC algorithm as follows.

The following second-order model (5.27) with disturbances and unmodeled dynamics (ρ) represents the experiment dynamics:

$$\begin{aligned} \dot{x}_1 &= x_2 \\ \dot{x}_2 &= a\,x_1 + \rho + h\,u \end{aligned} \tag{5.27}$$

Where ρ is a time-state function that represents the uncertainties of the system such as the non-linearity of the springs, the static friction, and the disturbances. The analysis of the ASMC is shown in the submitted article *sliding mode controllers for an adjustable stiffness wrist- elbow rehabilitator* (see appendix B).

5.5.1 Simulation asymptotic sliding mode controller

Figure 5.17 shows the desired trajectory (dotted red line) together with the output signal (continuous blue line). Figure 5.18 illustrates the behaviors of the tracking error (e_t) in magenta of the tracking error that varies according to $-1° \leq e_t \leq 1°$. It is highlighted that maximum values of this error correspond to ridges and valleys where the handle of the system is reversing the direction of rotation: clockwise-counterclockwise-clockwise and so on. The green line shows the control signal that represents the movement of the linear actuator stem.

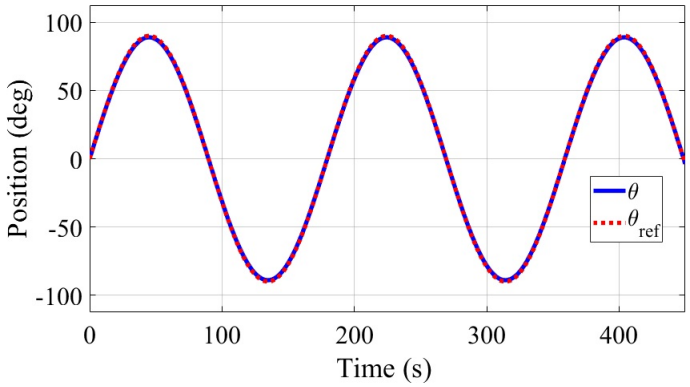

Figure 5.17: Handle position with ASMC.

5.6 SOMS Super-Twisting Controller

The ST controller is a robust and continuous control that uses the first derivative of the sliding variable and drives the sliding surface and its derivative to zero, this control avoids the chattering effect and rejects bounded perturbations.

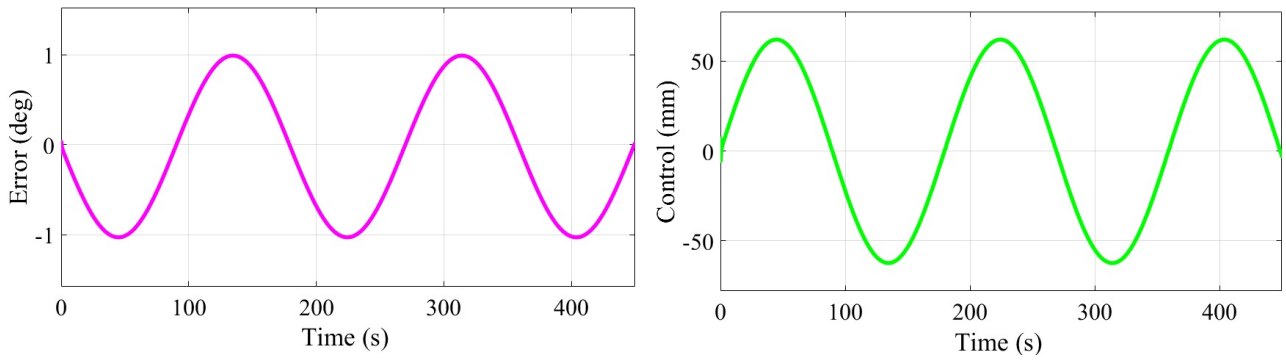

Figure 5.18: Error and control signal with ASMC.

Considering the system (5.27) the sliding surface s is defined as:

$$\begin{aligned} s &= (\dot{\theta}_d - x_2) + \lambda(\theta_d - x_1) \\ &= e_2 + \lambda\, e_1 \end{aligned} \tag{5.28}$$

Where θ_d is the angular position trajectory reference.

The analysis of stability and the proposal of the ST controller considering a Lyapunov function is shown in the submitted article *sliding mode controllers for an adjustable stiffness wrist- elbow rehabilitator* (see appendix B).

5.7 Simulation Results

This section reports the numerical results obtained from the simulation of the ST controller, it is tested by a tracking reference signal represented by a sinusoidal trajectory of the magnitude of 90 and frequency of 0.1 Hz.

Table 5.1: Control parameters.

Parameter	Value
α_1	550
α_2	100
δ	500
ϵ	1
Matrix P	$\begin{bmatrix} 800 & -75 \\ -75 & 8 \end{bmatrix}$

According to the five conditions mentioned in the submitted article *sliding mode controllers for an adjustable stiffness wrist- elbow rehabilitator*:

1. $\epsilon = 1 \Longrightarrow \alpha_1 = 750 > 2\epsilon,\ \alpha_2 = 200 > 0$
2. $P_{12} = -75 < 0$
3. $P_{11} = 800 > \dfrac{285625}{749} \approx 381.34$

4. $P_{22} = 8 > \dfrac{29}{22} \approx 1.318$

5. $P_{22}^2 + \epsilon P_{22} + P_{12} = -3 < 0$

Figure 5.19 shows the desired trajectory (dotted red line) together with the output signal (continuous blue line). Figure 5.20 illustrates the behaviors of the tracking error (e_t) in magenta the tracking error has smaller values than the ASMC strategy, except for an initial behavior where a variation in the interval [-1 °; 3 °] can be observed, the tracking error remains close to zero for the rest of the test. The green line shows the control signal that represents the movement of the linear actuator stem.

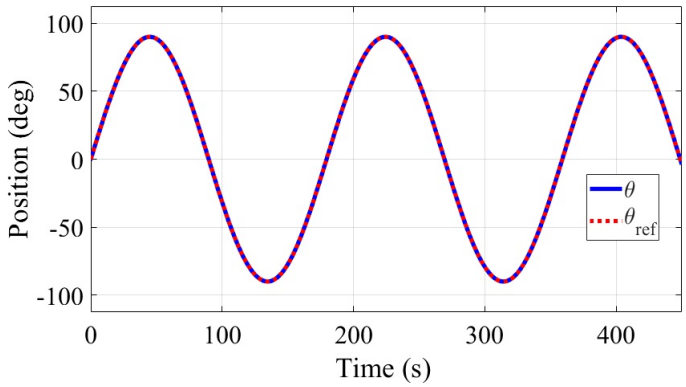

Figure 5.19: Handle position with ST.

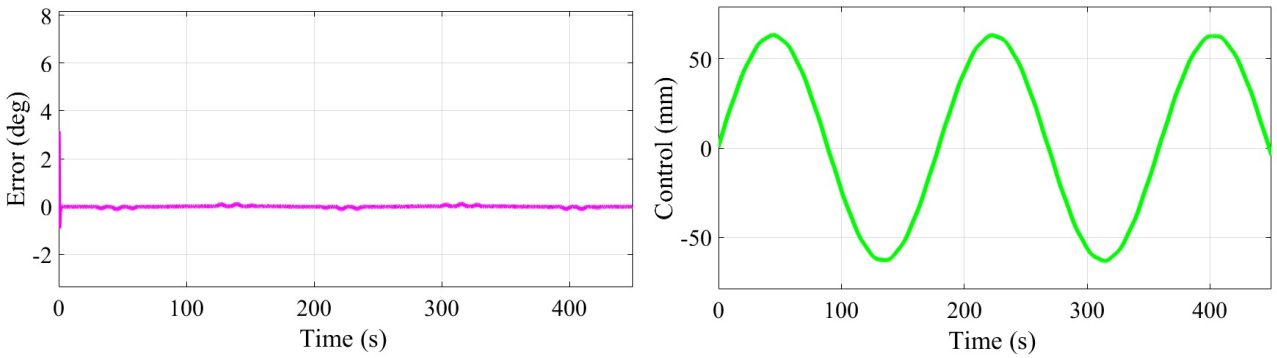

Figure 5.20: Error and control signal with ST.

5.8 Observer

Figure 5.21 shows the proposed configuration control where the control objective is considering the sliding surface s, the proposed controller combines a Super-Twisting Algorithm (STA) feedback control with a Generalized Variable Gain Super-Super-Twisting (VGSTA) Derivator used as State Observer which estimate $\dot{\theta}_d$.

From 5.16, this model can be expressed under the following state space form $[\theta, \dot{\theta}] = [x_1, x_2]$:

$$\begin{aligned} \dot{x}_1 &= x_2 \\ \dot{x}_2 &= a\,x_1 + b\,x_2 + h\,u \end{aligned} \tag{5.29}$$

The sliding surface (5.28) and the super-twisting control algorithm (**??**), a robust and exact derivative is proposed with convergence in finite time, by means of the STA or VGSTA

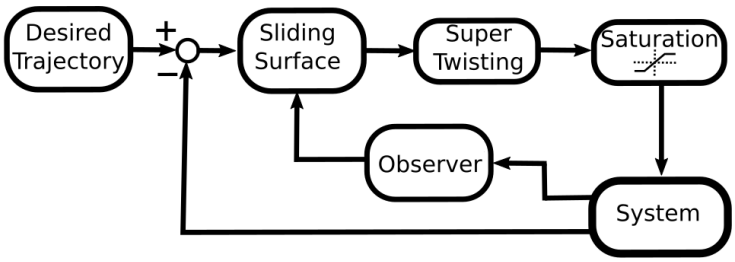

Figure 5.21: Control scheme with observer.

algorithm. If an input signal $x(t)$, which is defined in the interval $[0, \infty)$ and by measurement noise bounded with unknown characteristics and a base signal $x_0(t)$ with first derivative that has a global Lipschitz constant $L > 0$. The problem is to find a real-time estimate of $\dot{x}(t)$. The proposed VGSTA has the form:

$$\begin{aligned} \dot{\hat{x}}_1 &= \hat{x}_2 + z_1 \\ \dot{\hat{x}}_2 &= f(t, x_1, \hat{x}_2, u) + z_2 \end{aligned} \tag{5.30}$$

where $\hat{x}_1$ and $\hat{x}_2$ are the state estimates, while the correction variables z_1 and z_2 are the output error injection of the form:

$$z_1 = -k_1(t)\phi_1(\bar{x}_1) \tag{5.31}$$
$$z_2 = -k_2(t)\phi_2(\bar{x}_1) \tag{5.32}$$

the terms $\phi_{1,2}(\bar{x}_1)$, where $\bar{x}_1 = x_1 - \hat{x}_1$

$$\phi_1(\bar{x}_1) = |\bar{x}_1|^{1/2}\text{sign}(\bar{x}_1) + k_3\bar{x}_1 \tag{5.33}$$
$$\phi_2(\bar{x}_1) = \phi_1'(\bar{x}_1) = \frac{1}{2}\text{sign}(\bar{x}) + \frac{3}{2}k_3|\bar{x}_1|^{1/2}\text{sign}(\bar{x}_1) + k_3^2\bar{x}_1 \tag{5.34}$$

We have:

$$\dot{\hat{x}}_1 = -k_1(t)\phi_1(\hat{x}_1) + \hat{x}_2 \tag{5.35}$$
$$\dot{\hat{x}}_2 = -k_2(t)\phi_2(\hat{x}_1) \tag{5.36}$$

when $k_3 = 0$ and k_1, k_2 are constant, this algorithm becomes the STA. The additional k_3 term allows dealing with linear disturbances. If $k_3 \geq 0$ and $k_1(t)$ and $k_2(t)$ are:

$$\begin{aligned} k_1(t) &= \delta + \frac{1}{\beta}\left\{\frac{L(t)^2}{4\epsilon} + 2\epsilon L(t) + \epsilon + \epsilon(\beta + 4\epsilon)\right\} \\ k_2(t) &= \beta + 4\epsilon^2 + 2\epsilon k_1(t) \end{aligned} \tag{5.37}$$

where $\beta > 0$, $\epsilon > 0$, $\delta > 0$ are arbitrary constants and $L(t)$ is a known continuous function.

The existence of a constant $L > 0$ is guaranteed when the system states are bounded, then, the inequality:

$$|F(t, x_1, x_2, \hat{x}_2)| < L \tag{5.38}$$

If we consider the error as $e_1 = \hat{x}_1 - x(t)$, $e_2 = \hat{x}_2 - \dot{x}(t)$, it is obtained:

$$\dot{e}_1 = \dot{\hat{x}}_1 - \dot{x}(t) \tag{5.39}$$
$$\dot{e}_2 = \dot{\hat{x}}_2 - \ddot{x}(t) \tag{5.40}$$

The dynamic error is:

$$\dot{e}_1 = e_2 - k_1(t)\phi_1(e_1) \tag{5.41}$$
$$\dot{e}_2 = -k_2(t)\phi_2(e_1) - \ddot{x}(t) \tag{5.42}$$

where $|\ddot{x}(t)| \leq L(t)$, always that $L(t) > 0$, be a continuous function in $t \in [0, \tau)$, $\tau > 0$.

5.8.1 Simulation Results

The reported numerical results are shown in Fig. 5.22 from the controller (**??**) and the observer (5.30). The STA-VGSTA is tested under the control requirement which consists in tracking a reference signal represented by a sinusoidal trajectory of the magnitude of 90 and frequency of 0.035 Hz. Figure 5.22a shows the handle tracking performance with the ST controller, the tracking error (5.22b) is close to zero, except in the begging of the simulation and in the ridges and valleys of the input signal. The observer performance is shown in Fig. 5.22c and Fig. 5.22d, where the observer estimates the value of the rotational velocity of the handle (red line), as in tracking position (see Fig. 5.22a), the velocity estimation error are quickly steered to zero remains close to zero (see Fig. 5.22d), except for the simulation start where the error varies from -1.5 deg/s to 4.5 deg/s.

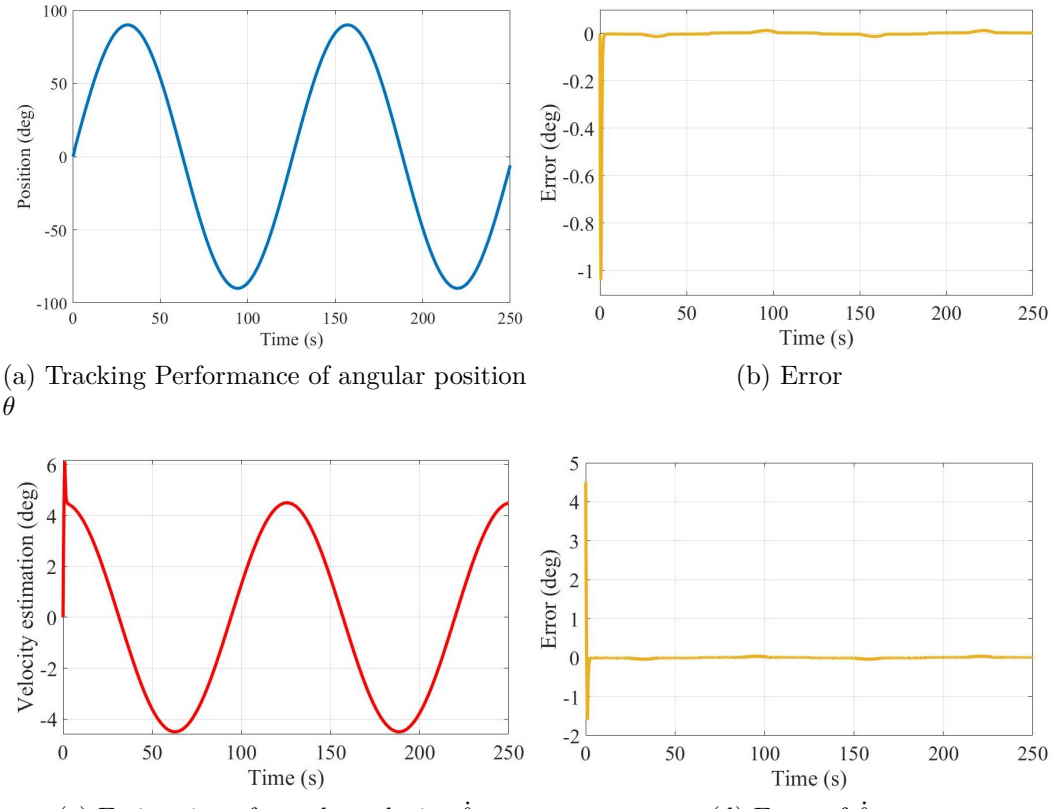

(a) Tracking Performance of angular position θ

(b) Error

(c) Estimation of angular velocity $\dot{\theta}$

(d) Error of $\dot{\theta}$

Figure 5.22: ST position control and VGSTA observer.

Chapter 6

Experimental results

The proposed linear actuator control is shown in Fig. 6.1, to get the accuracy of position (millimeters) it is used a PID controller, the NUCLEO STM32F767ZI microcontroller, an L298N motor driver is used to execute the control signal (PWM) and to switch the motor's direction, and an encoder is used to provide position feedback. The implementation code is considered to generate the PWM output using PID and sliding mode controllers.

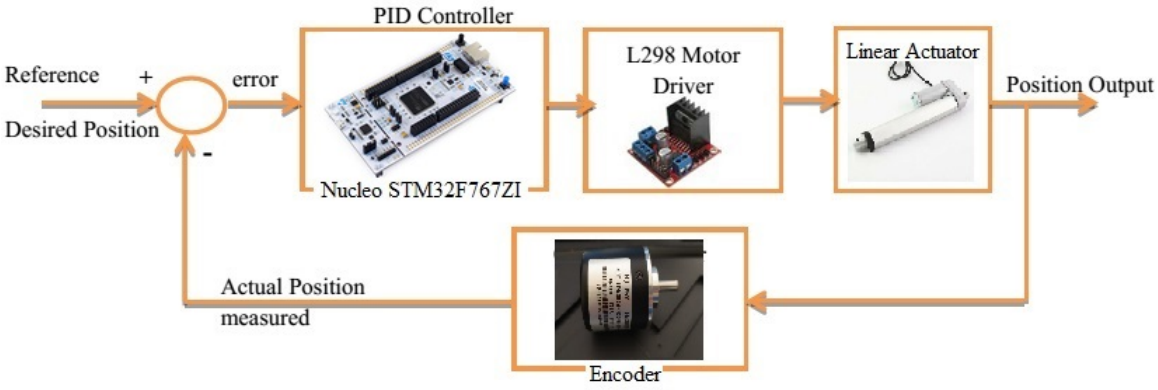

Figure 6.1: Linear motor control diagram.

Because the encoder pulses indicate a motor displacement, the motor speed can be approximated by a specific interval of time by calculating the number of pulses divided by the sample's time. With a maximum speed of 4.2 mm/s as can be seen in Fig. 6.2.

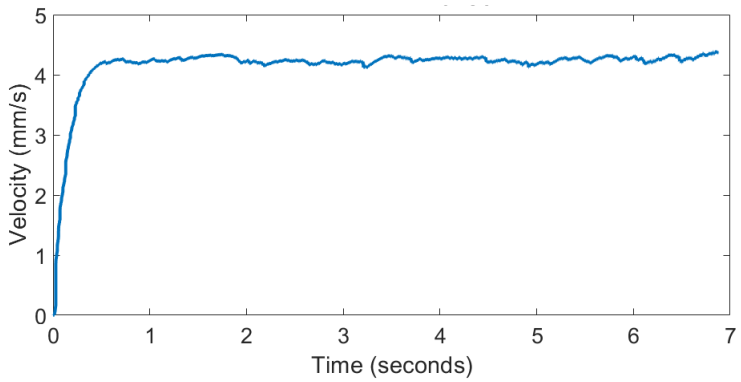

Figure 6.2: Linear motor response.

The first-order model approximates the linear motor model is:

$$\frac{\omega(s)}{V(s)} = \frac{0.83151}{1.867601s + 1} \tag{6.1}$$

Where the **fit of estimation** data is 90.61%, then the motor transfer function, where the system input will be represented by the voltage supply $V(s)$ and the output is the displacement $D(S)$ of the piston rod is:

$$\frac{D(S)}{V(S)} = \frac{0.83151}{1.867601s^2 + s} \tag{6.2}$$

6.1 Linear motor experimental results

The following points are important to be able to control linear actuators: 1) Adjusting the controller values and Simulink data reception sampling times and 2) Adjust the signal input with the restrictions of linear actuator length and maximum/minimum velocity.

Figure 6.3 shows the trajectory tracking of two signals, the rod of the linear actuator (output) must follow the reference signal, and a closed-loop control is performed as shown in Fig. 6.1.

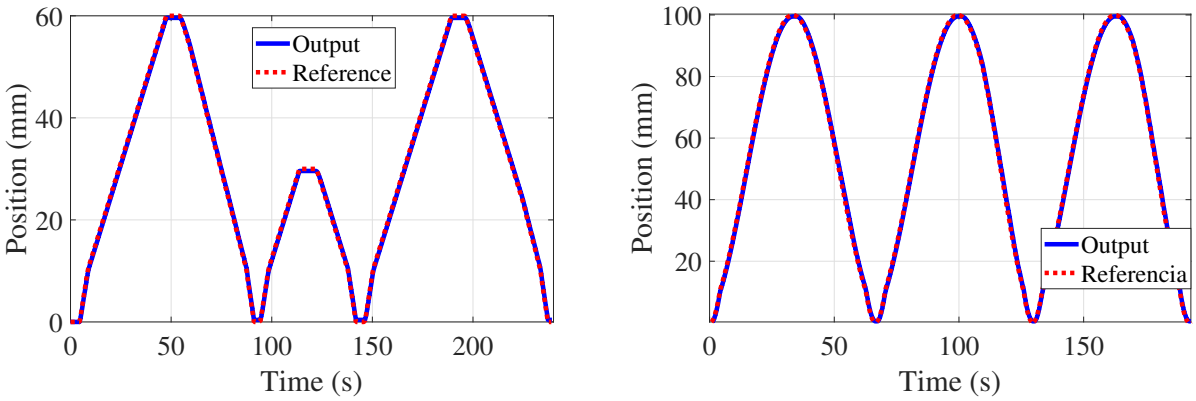

(a) Tracking trajectory 1.

(b) Tracking trajectory 2.

Figure 6.3: Control position based for 1 linear actuator.

Figure 6.4 shows the trajectory tracking of two signals, there is a reference signal (red), and the linear actuator 1 follows just the positive trajectory when the reference becomes negative the actuator remains at 0°. Linear actuator 2 follows the negative trajectory, when the reference returns to positive values actuator 2 remains at zero 0°.

Figures 6.3 and 6.4 show adequate trajectory tracking, according to the PID control and the linear actuator model (Eq. (6.2)), it is important to emphasize that in order to perform a tension adjustment and trajectory tracking in the rehabilitation system, the actuators must be completely controllable.

6.2 Open loop control

In the open-loop configuration, the control action (PID) is totally independent of the output of the system handle (θ). Figure 6.5 shows the system's configuration control:

The following experiments (Fig. 6.6 and Fig. 6.7) were carried out to see the system nature in an open-loop configuration, Fig. 6.6 shows the behavior of the adjustable stiffness device when it does not have springs, Fig. 6.6a shows the trajectory tracking, that despite good tracking, the error (see Fig. b) has maximums of ±5 degrees that occur when the trajectory reaches the 90° and -90°.

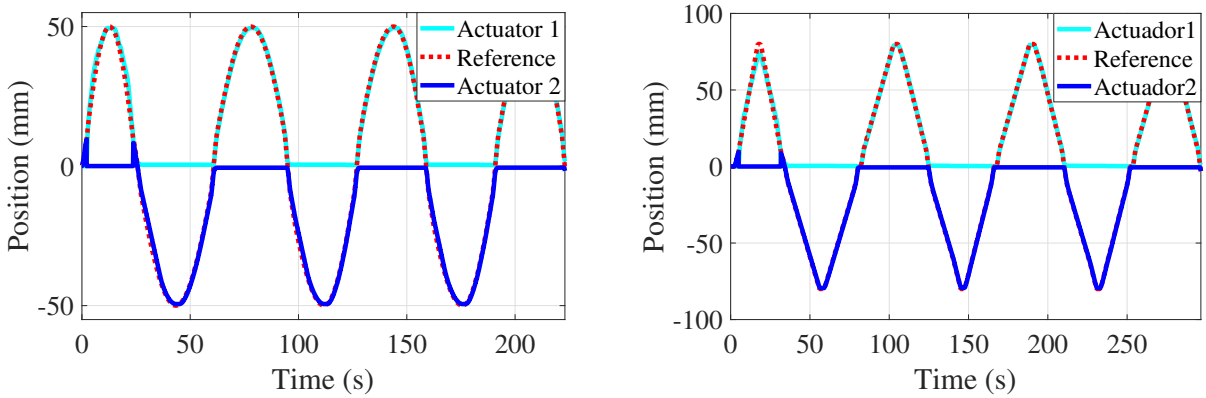

(a) Alternation tracking trajectory 1.

(b) Alternation tracking trajectory 1.

Figure 6.4: Control position for 2 linear actuators.

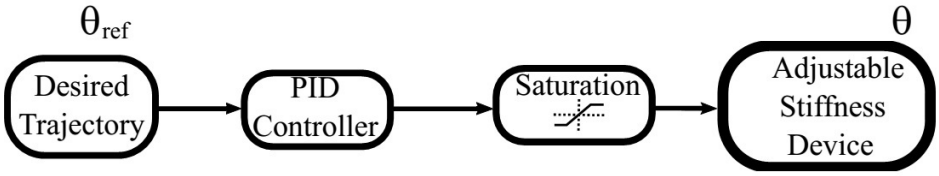

Figure 6.5: Open loop control scheme.

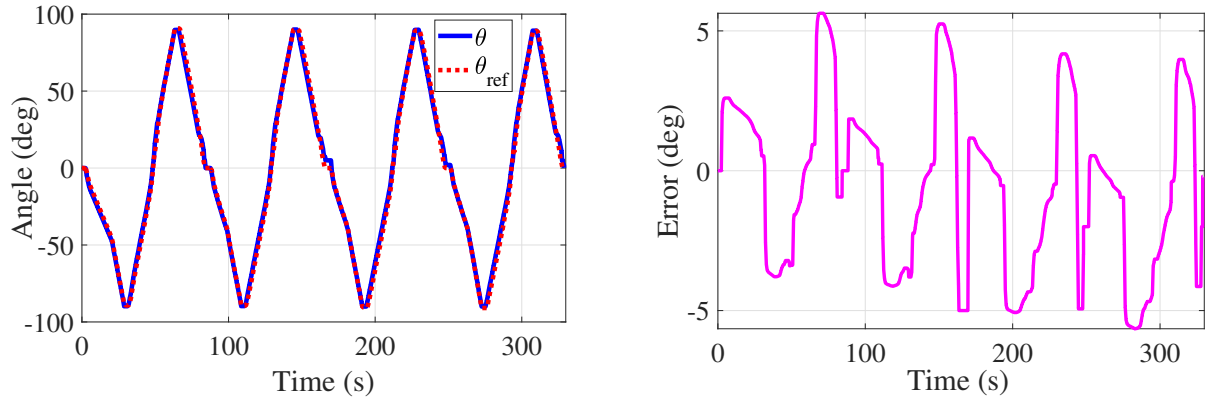

(a) Tracking trajectory.

(b) Error.

Figure 6.6: Control position open loop without springs.

Figure 6.7 shows the behavior of the system with the two springs with two different references (θ_{ref}). Figure 6.7a has as a reference a signal that goes from 90 to 90, with constant speed, while Fig. 6.7b has a sinusoidal reference, in which the speed varies. When introducing the springs to the system and since there is no feedback from the output, the behavior of the system is not favorable, since the tracking does not reach the highest points where it should go (90° and -90°). This behavior is more evident in Fig. 6.7b by having a sinusoidal signal as a reference.

6.3 Tension adjustment

Figure 6.8 shows the control proposal, it is divided into two parts, in Fig. 6.8a a trajectory tracking is carried out by the system from 0 s to 25 s where it reaches the desired trajectory, in this point is where the tension control intervenes from 25 s to 60 s, following a tension

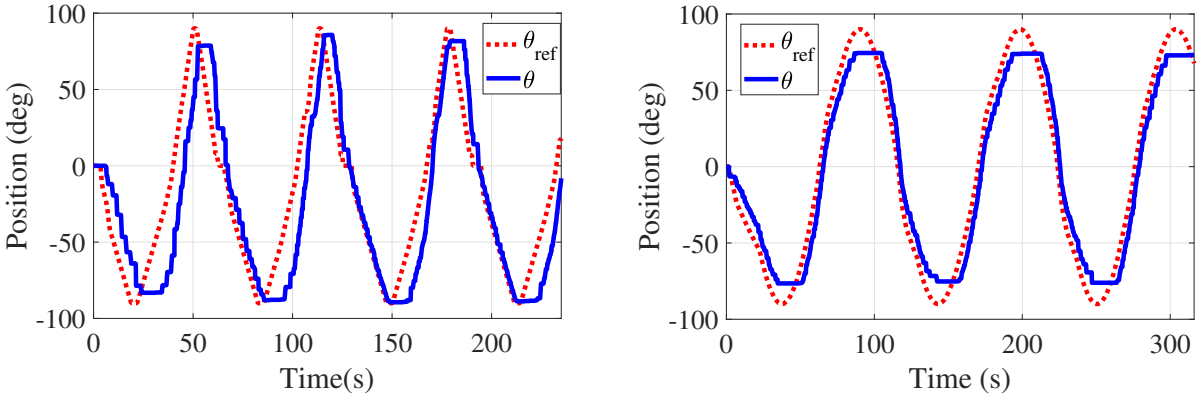

(a) Tracking trajectory 1.

(b) Tracking trajectory 2.

Figure 6.7: Control position open loop with springs.

modulation from 10 N to 25 N (see Figure 6.8b), this modulation leads to the handle having a deviation in its position.

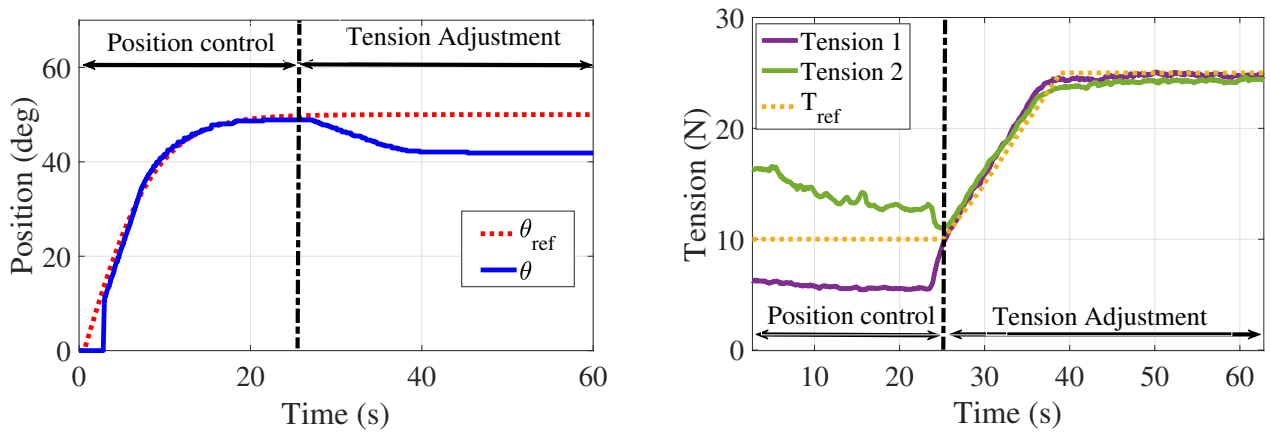

(a) Handle position.

(b) Tension behavior.

Figure 6.8: Position and tension adjustment technique.

Figure 6.9 shows the same technique performed as that of Fig. 6.8, in this test the tension adjustment is for 3 s every half cycle, and the results obtained are shown in Fig. 6.9a. Figure 6.9b shows the voltage peaks of Tension 2, showing an approximate tension of 23 N. Fig. 6.9c shows in more detail where the control modulation is performed while Fig. 6.9d shows the Average error divided into two parts the part, Error^+ is the positive trajectory and the Error^- that is the negative trajectory.

6.4 Experimental results with lineal controllers

The second-order differential equation that describes the motion of the rehabilitator device with viscous friction is delivered in Eq. (6.3).

$$\ddot{\theta} = c_1\theta + c_2\dot{\theta} + c_3 u \tag{6.3}$$

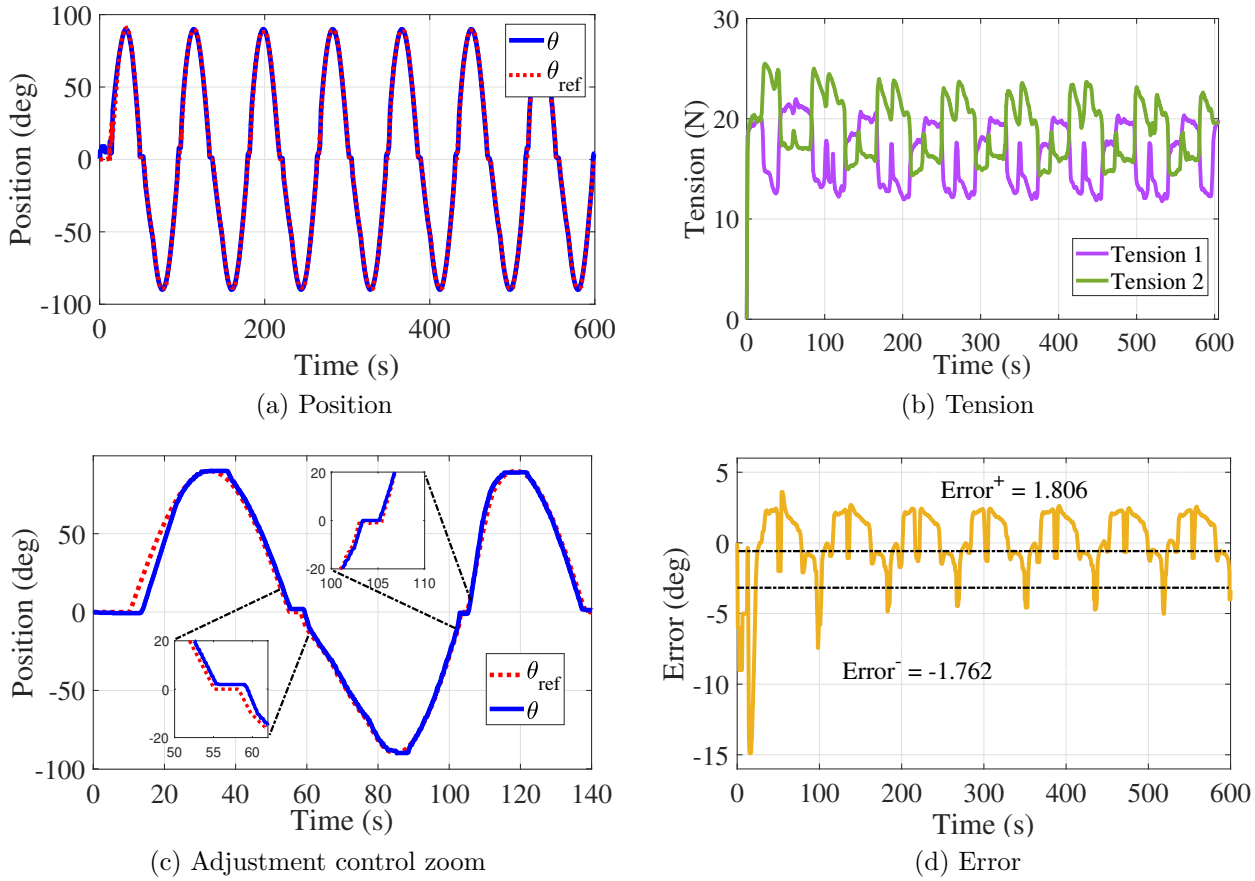

(a) Position (b) Tension

(c) Adjustment control zoom (d) Error

Figure 6.9: Control position and adjustment tension.

where $\dot{\theta} = \frac{d\theta}{dt}$, $\ddot{\theta} = \frac{d\dot{\theta}}{dt}$, c_1, c_2 and c_3 are physical parameters whose values are shown in Table 6.1. The control is generated by the mixed efforts of u_1 and u_2 of the two linear actuators as $u = u_1 - u_2$.

Table 6.1: Physical parameters.

Gain	Value	Units
c_1	-2403.80	deg/s^2
c_2	-439.56	deg/s
c_3	9772.10	deg/m s^2

Since supination-pronation rehabilitation exercises are a series of repetitive movements, with the same intensity and duration, the control informed in this thesis focuses on a trajectory-tracking problem. Then, a position-based tension control strategy is design with sinusoidal trajectories, with an amplitude of 90° and a frequency that can vary depending the patient's necessities. The Amplitude and frequency are adjusted with the help a physical therapist.

Fig 6.10 shows the control strategy with two linear controllers, the PD controller in charge of regulating the system's stiffness with tension measurement feedback provided by the load cells and the PID controller in charge of tracking regulation with angular position feedback measured by the encoder. The saturation block limits the action of controllers and motors, due to the physical restrictions of the system itself. According to the rehabilitation stage in which the patient is, the PD and PID controllers will switch to carry out the assigned task. Table 6.2 delivers the values of the gains for the PID controller and PD controller.

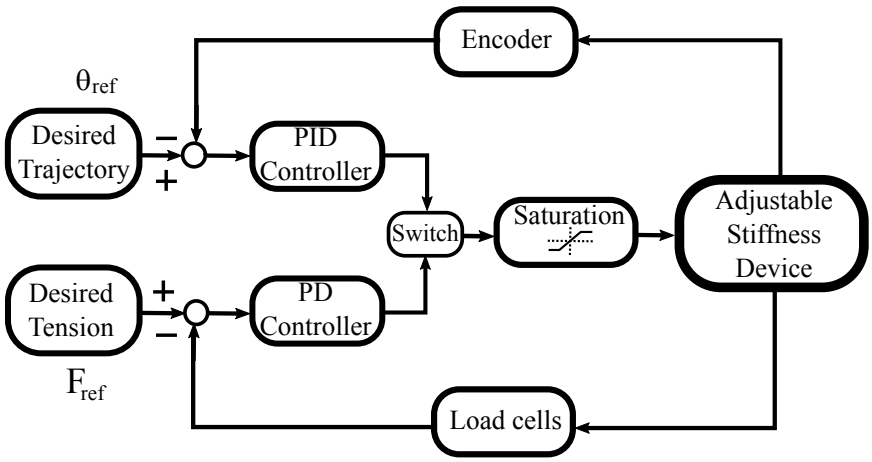

Figure 6.10: Control diagram [8].

Table 6.2: Gain values.

Gain	PID	PD
k_p	99.18	58.34
k_i	0.29	———
k_d	89.26	20.42

A series of experiments carried out on the adjustable stiffness device is shown in the article published in 2022 [8] as shown in Chapter 7, in which experiments were carried out for the three stages of rehabilitation: passive, active-assisted, and active. In the three cases, favorable results were shown, when the Tracking trajectory occurred (handle angular position), errors of less than 2% were achieved, and also when the system tension was adjusted, the springs and cables keep the desired value. A phenomenon occurred at the beginning of each experiment when the rehabilitator started, which took some time to react due to the springs, this phenomenon is due to the fact that the springs take some time to release the energy.

6.5 Experimental results with sliding mode controllers

The general idea of the sliding modes control strategies is illustrated in Fig. 6.11. But instead of PID and PD controller in this section is used the ASMC and the STA. To satisfy the passive and active phases of rehabilitation, the control strategy combines tension adjustment and trajectory tracking with two loops, one feedback for the tracking and the other for tension control by means of an encoder and load cells, respectively. Each control strategy (ASMC or STA) allows to alternate between the trajectory tracking control and the tension control using the switch observed in Fig. 6.11.

6.5.1 ASMC results

The experimental results obtained with ASMC and with the aim of emulating the full ROM for supination-pronation wrist-forearm **passive rehabilitation phase**, the reference is $\theta_{ref} = 90\sin(0.09t)$. The tracking reference is shown in Fig. 6.12a where good tracking can be observed. The tension evolution as the position change is shown in Fig. 6.12b. The mean tracking error of 2.07° can be observed in Fig. 6.12c.

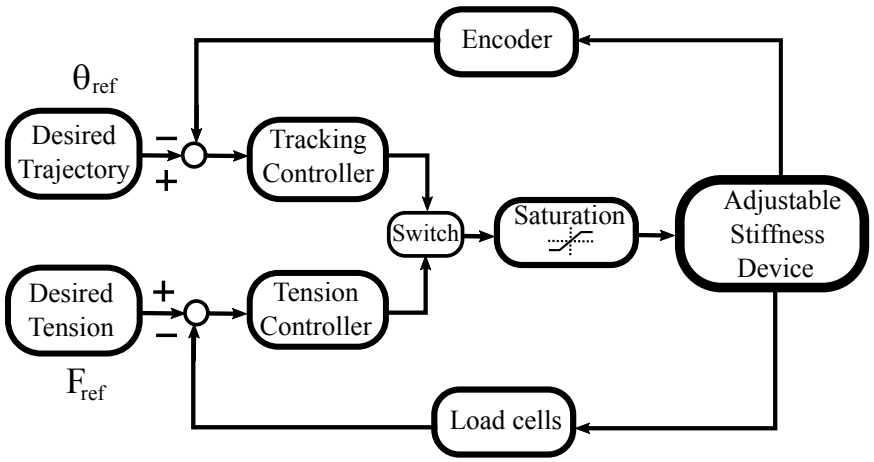

Figure 6.11: General control diagram

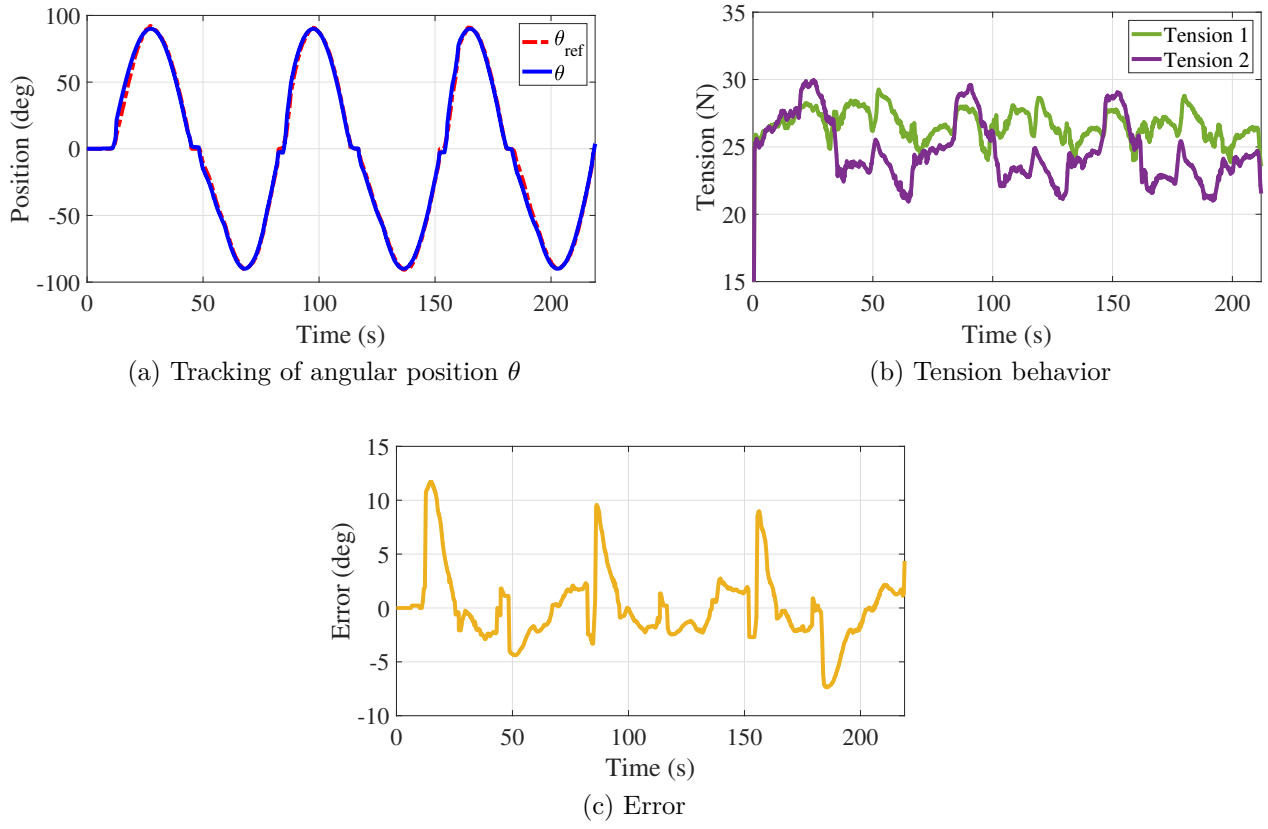

(a) Tracking of angular position θ

(b) Tension behavior

(c) Error

Figure 6.12: Trajectory tracking with tension adjustment, ASMC controller.

For the **active rehabilitation phase** the user performs the movement depending on his/her ROM, the adjustable stiffness rehabilitation device has a predefined torque that can be adjusted depending on the strength of the patient.

Figure 6.13a shows the angular position of the handle when the user performs the exercise, this movement can be carried out at the speed that the user can do it. The evolution of the tension is observed in Fig. 6.13b where they remain in a range due to torque restriction. The total torque with a reference value of 4.3 Nm is shown in Fig. 6.14.

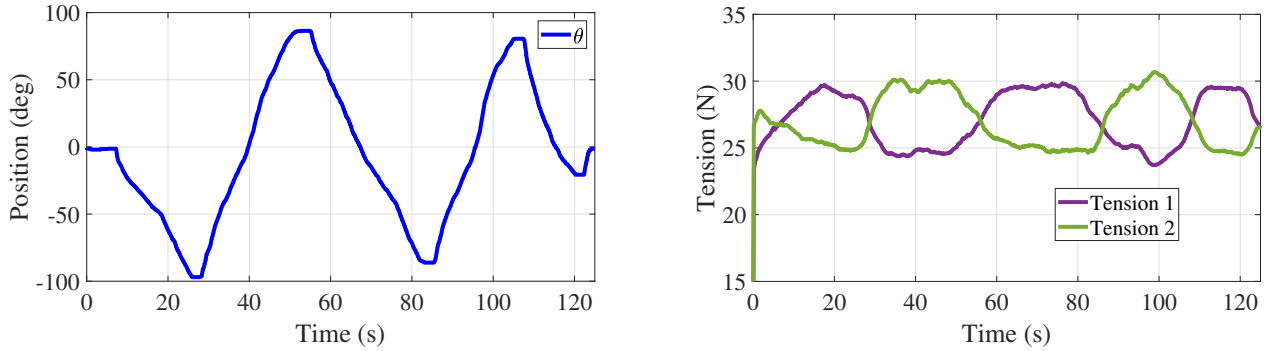

(a) Angular position θ (b) Tension behavior

Figure 6.13: Trajectory and tension behaviors with torque reference, ASMC controller.

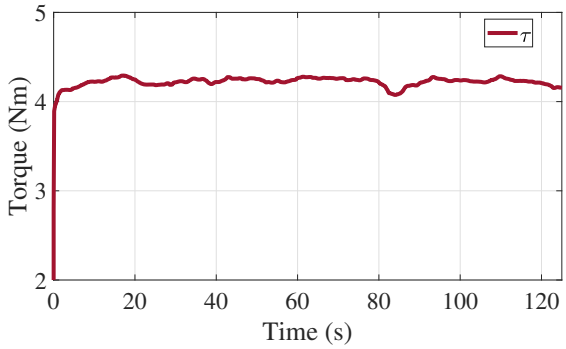

Figure 6.14: Total torque system, ASMC controller.

6.5.2 STA results

The STA is tested on the adjustable wrist-forearm physical rehabilitator obtaining results shown in Fig. 6.15. The tracking position turns out to be quite good along the entire trajectory except at the peaks and valleys of the sine wave (see Fig. 6.15a), the mean error in this experiment without tension adjustment is 2.3077°, which can be observed in Fig. 6.15b.

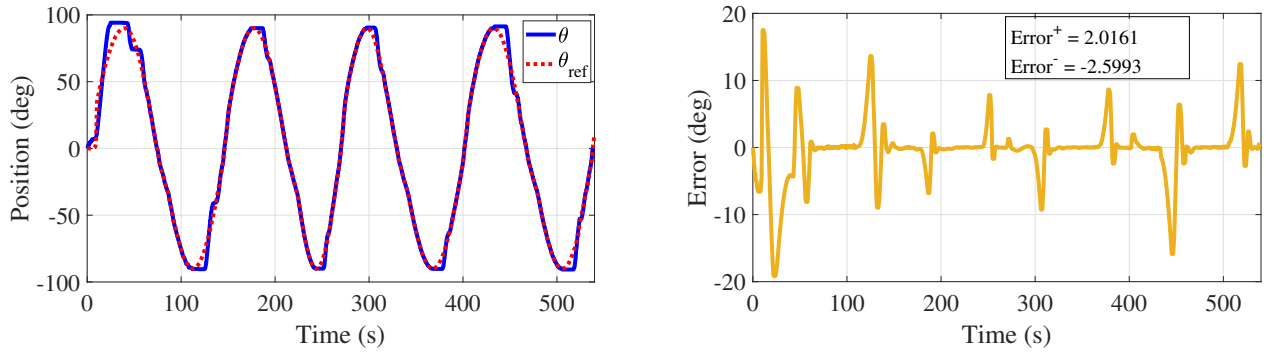

(a) Tracking position θ (b) Error

Figure 6.15: Position control without tension adjust, ST controller.

The following experiments are made with the same conditions established for the experimental test with the PID, PD, and ASMC strategies for the **passive rehabilitation phase**, which involve: reference trajectory and tension, the same time intervals for tension adjustment, and full supination-pronation ROM. First, the super-twisting controller is implemented

to track a reference trajectory and adjust the tension system (see Figures 6.16a and 6.16b). Super-twisting being a controller that is robust to bounded disturbances, it is expected to have a better performance than linear controllers (PID and PD), the tracking error which can be observed in Fig. 6.16c shows a lower mean error than the controllers presented above which is 1.486° which represents more than %50 improvements with respect to linear controllers.

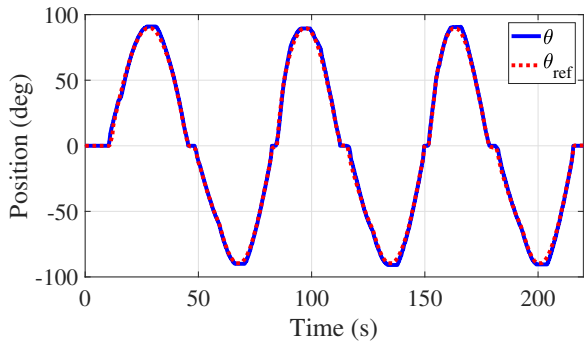

(a) Angular position θ

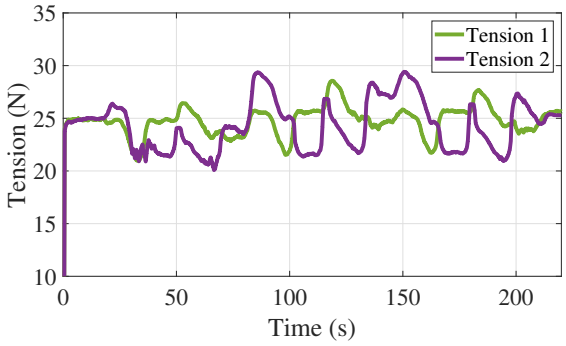

(b) Tension behavior

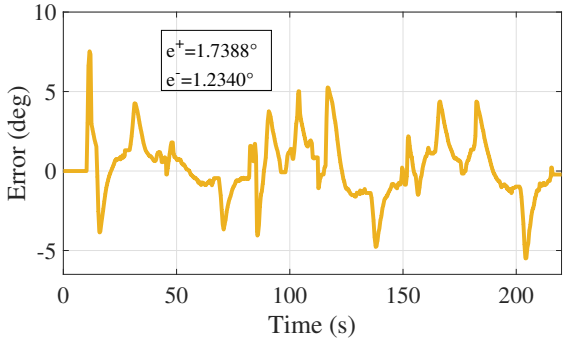

(c) Error

Figure 6.16: Trajectory and tension behaviors with load, ST controller.

For the **active rehabilitation phase** the user performs the supination-pronation movement at his/her own pace and ROM. Figure 6.17a reports the trajectory carried out which tries to emulate full ROM for a healthy person, Fig. 6.17b shows the tension evolution for the aforementioned trajectory, the two tensions remain in a range because the system torque requires to be constant.

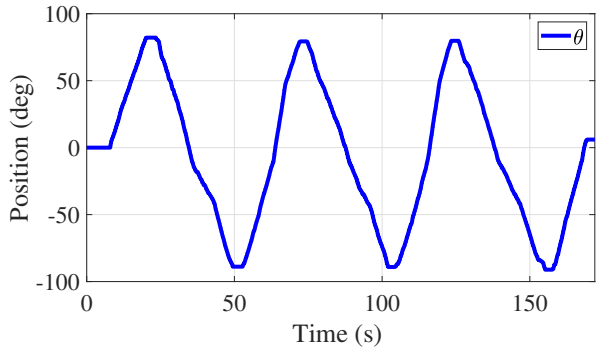

(a) Angular position θ

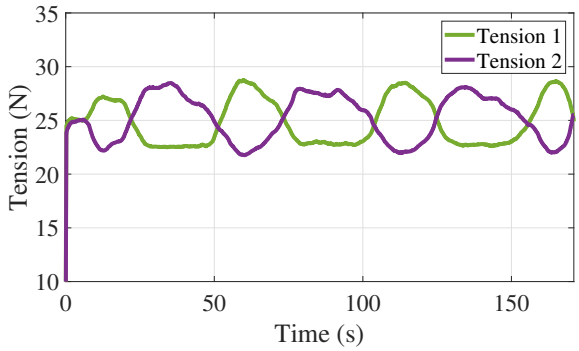

(b) Tension behavior

Figure 6.17: Trajectory and tension behaviors with torque reference, ST controller.

The total torque with a reference value of 3.6 Nm is shown in Fig. 6.18.

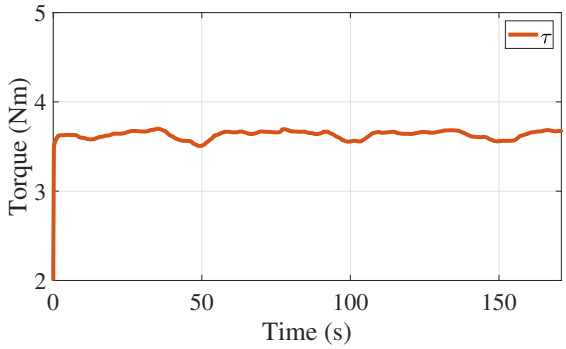

Figure 6.18: Total torque system, ST controller

The results show that emulating passive rehabilitation throughout the full ROM, results in a mean error of less than 3.6° for the four control strategies presented which represents less than 4% total error. The PID/PD controllers were the ones that obtained the highest mean error in the tests with 2.45°. This error is used for the comparison of the presented SMC strategies, with the ASMC, a 19.5% reduction of the error is obtained, with the ST/PD controller, the obtained reduction of the error is 28.27%, and finally, for the ST/ST controller, the error obtained had a 65.5% of improvement in relation to the PID/PD controllers.

Chapter 7

Conclusions

A new rehabilitation device has been reported in this thesis. This system is oriented to wrist-forearm supination-pronation exercises as part of rehabilitation protocols defined by physical therapists. The reported device is based on an adjustable stiffness approach to adapt torques to the medical conditions of potential patients. Based on experimental tests, the effectiveness of the rehabilitation device has been demonstrated, in addition, three control techniques have been tested for tracking and tension control which are responsible for carrying out the rehabilitation protocols.

Three main aspects have been validated: the effective trajectory tracking performed by the system, its capacity to regulate tensions in the cables, and its capacity to adjust the applied torque that represents the adjustment in the system stiffness. The execution of the wrist-forearm supination-pronation task, through several cycles, has been experimentally validated by contracting and releasing tension in the cables of the device by the control signals generated by two linear actuators.

The use of the adjustable stiffness rehabilitator reported in this paper in the passive, active-assisted, and in active phases of rehabilitation protocols has been demonstrated through experimental tests providing satisfactory results.

The control strategies proposed were proved experimentally assessed in terms of tracking trajectory and adjustable stiffness for the three phases of rehabilitation. Two linear control (PID and PD) and two continuous-time sliding modes controllers (asymptotic sliding mode and super-twisting) have been implemented and tested for a set of real-time experiments. Linear controllers have proven to be more effective in tension adjustment while sliding mode controllers present high accuracy when tracking the angular position of the device's handle or in the combined action of position and tension scenario. The obtained experimental results place the two SMC strategies as excellent candidates to perform the tasks aimed at the rehabilitation of the forearm-wrist supination-pronation motion. Based on the experimental results reported in this thesis, it can be established that the super twisting controller possesses better performance for both scenarios with and without the presence of external disturbances.

Future work:

- Design a simultaneous strategy control of tracking and tension adjustment.
- Improve the design of the prototype, in the aesthetic aspect as well as in the reduction of friction in its components.
- Carry out tests with patients who are undergoing forearm-wrist rehabilitation to assess the effectiveness of the system.

- Characterize the appropriate torques, forces, and speeds to accomplish an appropriate rehabilitation process, both in passive and active phases.

Appendix A

Published article

Adjustable stiffness-based supination-pronation forearm physical rehabilitator

- Posted on June 17, 2022,
- In the Journal of Applied Sciences, https://doi.org/ 10.3390/app12126164.

applied sciences

MDPI

Article

Adjustable Stiffness-Based Supination–Pronation Forearm Physical Rehabilitator

Adrian Camacho-Ramirez [1], Juan Carlos Ávila-Vilchis [1,*], Belem Saldivar [2], Adriana H. Vilchis-González [1] and Juan Manuel Jacinto-Villegas [1,3]

[1] Faculty of Engineering, Universidad Autonoma del Estado de México, Toluca 50130, Mexico; acamachor004@alumno.uaemex.mx (A.C.-R.); avilchisg@uaemex.mx (A.H.V.-G.); jmjacintov@uaemex.mx (J.M.J.-V.)
[2] Department of Automatic Control, CINVESTAV-IPN, Av. Instituto Politécnico Nacional 2508, Mexico City 07360, Mexico; msaldivar@ctrl.cinvestav.mx
[3] Programa Investigadoras e Investigadores por México del CONACYT, Av. Insurgentes Sur 1582, Col. Crédito Constructor, Alcaldía Benito Juárez, Mexico City 03940, Mexico
* Correspondence: jcavilav@uaemex.mx

Figure A.1: Heading of the published work.

Appendix B

Submitted article

Sliding mode controllers for an adjustable stiffness wrist-elbow rehabilitator

- Submitted on January 25, 2023,
- In the International Journal of Control, Automation and Systems

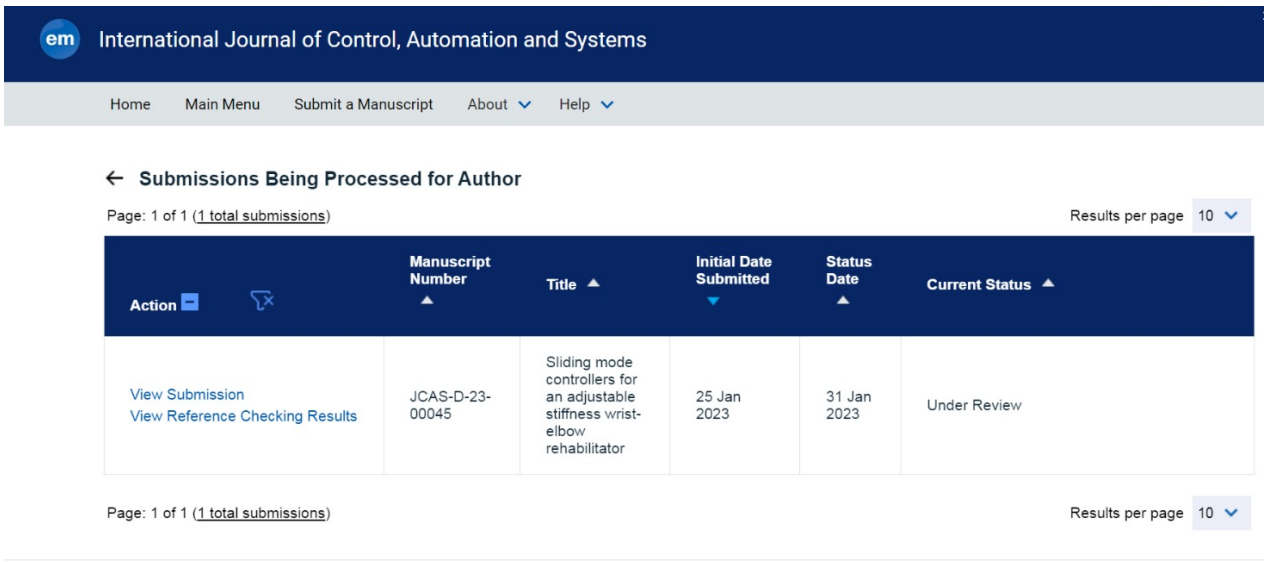

Figure B.1: Heading of the submitted work.

Appendix C

Experimental platform

Construction of the experimental platform.

Throughout this project, a prototype of the forearm-wrist rehabilitator was made as shown in Chapter 4 and 5, where the proposed control strategies and the experiments carried out for the three forearm-wrist pronation and supination rehabilitation protocols are validated.

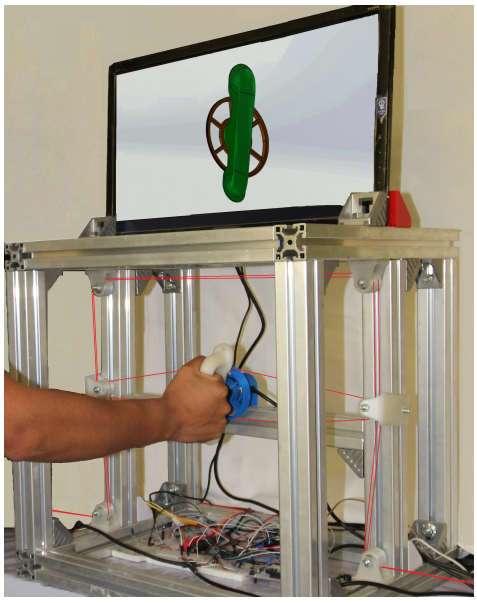

Figure C.1: Experimental platform.

Bibliography

[1] R. E. Skelton and M. C. de Oliveira, *Tensegrity systems*, vol. 1. Springer, 2009.

[2] J. F. Farrell and H. B. Hoffman, "Dynamic hand splint," Oct. 13 2009. US Patent 7,601,130.

[3] G. Rosati, P. Gallina, and S. Masiero, "Design, implementation and clinical tests of a wire-based robot for neurorehabilitation," *IEEE Transactions on Neural Systems and Rehabilitation Engineering*, vol. 15, no. 4, pp. 560–569, 2007.

[4] S. R. Lessard, *The Design, Construction, and Evaluation of Crux: A Tensegrity-Inspired Compliant Robotic Upper-Extremity Exosuit*. PhD thesis, UC Santa Cruz, 2018.

[5] C. Kisner, L. A. Colby, and J. Borstad, *Therapeutic exercise: foundations and techniques*. Fa Davis, 2017.

[6] C. H. Taboadela, "Goniometría," *Una herramienta para la evaluación de las incapacidades laborales. Buenos Aires: Asociart ART*, 2007.

[7] TheraBand, "Thera-band trusted color progression." url https://www.therabandclx.com/extras/force-chart, 2019. Accessed 22-03-2019.

[8] A. Camacho-Ramirez, J. C. Ávila-Vilchis, B. Saldivar, A. H. Vilchis-González, and J. M. Jacinto-Villegas, "Adjustable stiffness-based supination–pronation forearm physical rehabilitator," *Applied Sciences*, vol. 12, no. 12, p. 6164, 2022.

[9] INEGI, "Discapacidad en mexico." url http://internet.contenidos.inegi.org.mx/contenidos/ productos/prodserv/contenidos/espanol/bv-inegi/productos/nuevaestruc/702825090203.pdf., 2015. Accedido 22-10-2018.

[10] S. Wolf, T. Bahls, M. Chalon, W. Friedl, M. Grebenstein, H. Höppner, M. Kühne, D. Lakatos, N. Mansfeld, M. C. Özparpucu, *et al.*, "Soft robotics with variable stiffness actuators: Tough robots for soft human robot interaction," in *Soft robotics*, pp. 231–254, Springer, 2015.

[11] A. Verl, A. Albu-Schäffer, O. Brock, and A. Raatz, *Soft Robotics*. Springer, 2015.

[12] S. Wolf, G. Grioli, O. Eiberger, W. Friedl, M. Grebenstein, H. Höppner, E. Burdet, D. G. Caldwell, R. Carloni, M. G. Catalano, *et al.*, "Variable stiffness actuators: Review on design and components," *IEEE/ASME transactions on mechatronics*, vol. 21, no. 5, pp. 2418–2430, 2015.

[13] R. Motro, *Tensegrity: structural systems for the future*. Elsevier, 2003.

[14] F. R. Buckminster, "Tensile-integrity structures," Nov. 13 1962. US Patent 3,063,521.

[15] C. Gosselin, P. Cardou, T. Bruckmann, and A. Pott, *Cable-Driven Parallel Robots: Proceedings of the Third International Conference on Cable-Driven Parallel Robots*, vol. 53. Springer, 2017.

[16] Q. Boehler, S. Abdelaziz, M. Vedrines, P. Poignet, and P. Renaud, "From modeling to control of a variable stiffness device based on a cable-driven tensegrity mechanism," *Mechanism and Machine Theory*, vol. 107, pp. 1–12, 2017.

[17] S. Lessard, J. Bruce, E. Jung, M. Teodorescu, V. SunSpiral, and A. Agogino, "A lightweight, multi-axis compliant tensegrity joint," in *Robotics and Automation (ICRA), 2016 IEEE International Conference on*, pp. 630–635, IEEE, 2016.

[18] S. M. Levin, *Tensegrity: the new biomechanics*, vol. 9. Oxford University Press, Oxford, 2015.

[19] M. Hutson and A. Ward, *Oxford textbook of musculoskeletal medicine*. Oxford University Press, 2015.

[20] R. Connelly and W. Whiteley, "Second-order rigidity and prestress stability for tensegrity frameworks," *SIAM Journal on Discrete Mathematics*, vol. 9, no. 3, pp. 453–491, 1996.

[21] S. D. Guest, "The stiffness of tensegrity structures," *IMA Journal of Applied Mathematics*, vol. 76, no. 1, pp. 57–66, 2010.

[22] S. H. Juan and J. M. M. Tur, "Tensegrity frameworks: static analysis review," *Mechanism and Machine Theory*, vol. 43, no. 7, pp. 859–881, 2008.

[23] A. P. Sabelhaus, J. Bruce, K. Caluwaerts, P. Manovi, R. F. Firoozi, S. Dobi, A. M. Agogino, and V. SunSpiral, "System design and locomotion of superball, an untethered tensegrity robot," in *Robotics and Automation (ICRA), 2015 IEEE International Conference on*, pp. 2867–2873, IEEE, 2015.

[24] C. Sultan and R. Skelton, "Deployment of tensegrity structures," *International Journal of Solids and Structures*, vol. 40, no. 18, pp. 4637–4657, 2003.

[25] J. Aldrich, R. Skelton, and K. Kreutz-Delgado, "Control synthesis for a class of light and agile robotic tensegrity structures," in *Proceedings of the 2003 American Control Conference, 2003.*, vol. 6, pp. 5245–5251, IEEE, 2003.

[26] V. SunSpiral, G. Gorospe, J. Bruce, A. Iscen, G. Korbel, S. Milam, A. Agogino, and D. Atkinson, "Tensegrity based probes for planetary exploration: Entry, descent and landing (edl) and surface mobility analysis," *International Journal of Planetary Probes*, vol. 7, 2013.

[27] A. Tibert and S. Pellegrino, "Review of form-finding methods for tensegrity structures," *International Journal of Space Structures*, vol. 26, no. 3, pp. 241–255, 2011.

[28] A. P. Sabelhaus, H. Ji, P. Hylton, Y. Madaan, C. Yang, A. M. Agogino, J. Friesen, and V. SunSpiral, "Mechanism design and simulation of the ultra spine: a tensegrity robot," in *ASME 2015 International Design Engineering Technical Conferences and Computers and Information in Engineering Conference*, pp. V05AT08A059–V05AT08A059, American Society of Mechanical Engineers, 2015.

[29] S. Lessard, P. Pansodtee, A. Robbins, L. B. Baltaxe-Admony, J. M. Trombadore, M. Teodorescu, A. Agogino, and S. Kurniawan, "Crux: A compliant robotic upper-extremity exosuit for lightweight, portable, multi-joint muscular augmentation," in *Rehabilitation Robotics (ICORR), 2017 International Conference on*, pp. 1633–1638, IEEE, 2017.

[30] T. Bruckmann and A. Pott, *Cable-driven parallel robots*, vol. 12. Springer, 2012.

[31] D. Surdilovic and R. Bernhardt, "String-man: a new wire robot for gait rehabilitation," in *Robotics and Automation, 2004. Proceedings. ICRA'04. 2004 IEEE International Conference on*, vol. 2, pp. 2031–2036, IEEE, 2004.

[32] C. Sultan and R. Skelton, "Integrated design of controllable tensegrity structures," *Adaptive structures and material systems-1997*, pp. 27–35, 1997.

[33] G. Antonelli, F. Arrichiello, F. Caccavale, and A. Marino, "A decentralized controller-observer scheme for multi-agent weighted centroid tracking," *IEEE Transactions on Automatic Control*, vol. 58, no. 5, pp. 1310–1316, 2013.

[34] M. A. Khosravi and H. D. Taghirad, "Robust pid control of fully-constrained cable driven parallel robots," *Mechatronics*, vol. 24, no. 2, pp. 87–97, 2014.

[35] B. T. Mirletz, R. D. Quinn, and V. SunSpiral, "Cpgs for adaptive control of spine-like tensegrity structures," in *Proceedings of 2015 International Conference on Robotics and Automation (ICRA2015) Workshop on Central Pattern Generators for Locomotion Control: Pros, Cons & Alternatives*, 2015.

[36] V. Utkin, J. Guldner, and M. Shijun, *Sliding mode control in electro-mechanical systems*, vol. 34. CRC press, 1999.

[37] Y. Shtessel, C. Edwards, L. Fridman, and A. Levant, *Sliding mode control and observation*, vol. 10. Springer, 2014.

[38] A. Levant, "Sliding order and sliding accuracy in sliding mode control," *International journal of control*, vol. 58, no. 6, pp. 1247–1263, 1993.

[39] A. Levant, "Robust exact differentiation via sliding mode technique," *automatica*, vol. 34, no. 3, pp. 379–384, 1998.

[40] A. Swikir and V. Utkin, "Chattering analysis of conventional and super twisting sliding mode control algorithm," in *2016 14th international workshop on variable structure systems (VSS)*, pp. 98–102, IEEE, 2016.

[41] J. A. Moreno and M. Osorio, "A lyapunov approach to second-order sliding mode controllers and observers," in *2008 47th IEEE conference on decision and control*, pp. 2856–2861, IEEE, 2008.

[42] J. A. Moreno, "A linear framework for the robust stability analysis of a generalized super-twisting algorithm," in *2009 6th International Conference on Electrical Engineering, Computing Science and Automatic Control (CCE)*, pp. 1–6, IEEE, 2009.

[43] A. Dávila, J. A. Moreno, and L. Fridman, "Optimal lyapunov function selection for reaching time estimation of super twisting algorithm," in *Proceedings of the 48h IEEE Conference on Decision and Control (CDC) held jointly with 2009 28th Chinese Control Conference*, pp. 8405–8410, IEEE, 2009.

[44] A. G. Rovira and J. M. M. Tur, "Control and simulation of a tensegrity-based mobile robot," *Robotics and Autonomous Systems*, vol. 57, no. 5, pp. 526–535, 2009.

[45] C. Nagavani, "Textbook of biomechanics and exercise therapy," *Dilshuknagar, Hyderabad*, 2003.

[46] J. R. Andrews, G. L. Harrelson, K. E. Wilk, *et al.*, *Physical Rehabilitation of the Injured Athlete: Expert Consult-Online and Print*. Elsevier Health Sciences, 2012.

[47] K. E. Wilk, T. S. Ellenbecker, and L. C. Macrina, "Rehabilitation of the overhead athlete's elbow," in *Elbow Ulnar Collateral Ligament Injury*, pp. 227–259, Springer, 2015.

[48] C. E. Giangarra and R. C. Manske, *Clinical Orthopaedic Rehabilitation: A Team Approach E-book*. Elsevier Health Sciences, 2017.

[49] W. H. Organization *et al.*, *WHO global disability action plan 2014-2021: Better health for all people with disability*. World Health Organization, 2015.

[50] W. J. Nusselder, C. C. Looman, H. Van Oyen, and R. T. D. C. Yokota, "Attributing causes to disability," in *International Handbook of Health Expectancies*, vol. 9, pp. 87–105, Springer, 2020.

[51] W. H. Organization *et al.*, *World report on disability*. World Health Organization, 2011.

[52] C. Senanayake and S. A. Senanayake, "Emerging robotics devices for therapeutic rehabilitation of the lower extremity," in *2009 IEEE/ASME International Conference on Advanced Intelligent Mechatronics*, pp. 1142–1147, IEEE, 2009.

[53] A. Alamdari and V. Krovi, "Design and analysis of a cable-driven articulated rehabilitation system for gait training," *Journal of Mechanisms and Robotics*, vol. 8, no. 5, p. 051018, 2016.

[54] C. Bütefisch, H. Hummelsheim, P. Denzler, and K.-H. Mauritz, "Repetitive training of isolated movements improves the outcome of motor rehabilitation of the centrally paretic hand," *Journal of the neurological sciences*, vol. 130, no. 1, pp. 59–68, 1995.

[55] M. A. Padilla-Castañeda, E. Sotgiu, M. Barsotti, A. Frisoli, P. Orsini, A. Martiradonna, C. Laddaga, and M. Bergamasco, "An orthopaedic robotic-assisted rehabilitation method of the forearm in virtual reality physiotherapy," *Journal of healthcare engineering*, vol. 2018, 2018.

[56] G. Saposnik, L. G. Cohen, M. Mamdani, S. Pooyania, M. Ploughman, D. Cheung, J. Shaw, J. Hall, P. Nord, S. Dukelow, *et al.*, "Efficacy and safety of non-immersive virtual reality exercising in stroke rehabilitation (evrest): a randomised, multicentre, single-blind, controlled trial," *The Lancet Neurology*, vol. 15, no. 10, pp. 1019–1027, 2016.

[57] S. M. Hatem, G. Saussez, M. della Faille, V. Prist, X. Zhang, D. Dispa, and Y. Bleyenheuft, "Rehabilitation of motor function after stroke: a multiple systematic review focused on techniques to stimulate upper extremity recovery," *Frontiers in human neuroscience*, vol. 10, p. 442, 2016.

[58] R. Bertani, C. Melegari, C. Maria, A. Bramanti, P. Bramanti, and R. S. Calabrò, "Effects of robot-assisted upper limb rehabilitation in stroke patients: a systematic review with meta-analysis," *Neurological Sciences*, vol. 38, no. 9, pp. 1561–1569, 2017.

[59] P. K. Jamwal, S. Hussain, M. H. Ghayesh, and S. V. Rogozina, "Impedance control of an intrinsically compliant parallel ankle rehabilitation robot," *IEEE Transactions on Industrial Electronics*, vol. 63, no. 6, pp. 3638–3647, 2016.

[60] C. Duret, A.-G. Grosmaire, and H. I. Krebs, "Robot-assisted therapy in upper extremity hemiparesis: overview of an evidence-based approach," *Frontiers in Neurology*, vol. 10, p. 412, 2019.

[61] R. Gassert and V. Dietz, "Rehabilitation robots for the treatment of sensorimotor deficits: a neurophysiological perspective," *Journal of neuroengineering and rehabilitation*, vol. 15, no. 1, p. 46, 2018.

[62] "Medical dictionary." Available http://medical-dictionary.thefreedictionary.com/. Accessed 29-05-2019.

[63] S. Lum, S. L. Lehman, and D. J. Reinkensmeyer, "The bimanual lifting rehabilitator: an adaptive machine for therapy of stroke patients," *IEEE Transactions on Rehabilitation Engineering*, vol. 3, no. 2, pp. 166–174, 1995.

[64] H. I. Krebs, N. Hogan, M. L. Aisen, and B. T. Volpe, "Robot-aided neurorehabilitation," *IEEE transactions on rehabilitation engineering*, vol. 6, no. 1, pp. 75–87, 1998.

[65] S. K. Charles, H. I. Krebs, B. T. Volpe, D. Lynch, and N. Hogan, "Wrist rehabilitation following stroke: initial clinical results," in *9th International Conference on Rehabilitation Robotics, 2005. ICORR 2005.*, pp. 13–16, IEEE, 2005.

[66] L. E. Kahn, M. L. Zygman, W. Z. Rymer, and D. J. Reinkensmeyer, "Robot-assisted reaching exercise promotes arm movement recovery in chronic hemiparetic stroke: a randomized controlled pilot study," *Journal of neuroengineering and rehabilitation*, vol. 3, no. 1, p. 12, 2006.

[67] F. Amirabdollahian, R. Loureiro, E. Gradwell, C. Collin, W. Harwin, and G. Johnson, "Multivariate analysis of the fugl-meyer outcome measures assessing the effectiveness of gentle/s robot-mediated stroke therapy," *Journal of NeuroEngineering and Rehabilitation*, vol. 4, no. 1, p. 4, 2007.

[68] J. Furusho, N. Shichi, X. Hu, T. Kikuchi, K. Nakayama, C. Li, Y. Yamaguchi, A. Inoue, and U. Ryu, "Development of a 6-dof force display system with high safety and its application to rehabilitation," in *2006 International Conference on Mechatronics and Automation*, pp. 962–967, IEEE, 2006.

[69] J. He, E. Koeneman, R. Schultz, D. Herring, J. Wanberg, H. Huang, T. Sugar, R. Herman, and J. Koeneman, "Rupert: a device for robotic upper extremity repetitive therapy," in *2005 IEEE Engineering in Medicine and Biology 27th Annual Conference*, pp. 6844–6847, IEEE, 2006.

[70] H. Zhang, H. Austin, S. Buchanan, R. Herman, J. Koeneman, and J. He, "Feasibility study of robot-assisted stroke rehabilitation at home using rupert," in *The 2011 IEEE/ICME International Conference on Complex Medical Engineering*, pp. 604–609, IEEE, 2011.

[71] J. C. Perry, J. Rosen, and S. Burns, "Upper-limb powered exoskeleton design," *IEEE/ASME transactions on mechatronics*, vol. 12, no. 4, pp. 408–417, 2007.

[72] A. U. Pehlivan, O. Celik, and M. K. O'Malley, "Mechanical design of a distal arm exoskeleton for stroke and spinal cord injury rehabilitation," in *2011 IEEE International Conference on Rehabilitation Robotics*, pp. 1–5, IEEE, 2011.

[73] S. J. Ball, I. E. Brown, and S. H. Scott, "Medarm: a rehabilitation robot with 5dof at the shoulder complex," in *2007 IEEE/ASME international conference on Advanced intelligent mechatronics*, pp. 1–6, IEEE, 2007.

[74] T. Nef, M. Mihelj, and R. Riener, "Armin: a robot for patient-cooperative arm therapy," *Medical & biological engineering & computing*, vol. 45, no. 9, pp. 887–900, 2007.

[75] A. U. Pehlivan, F. Sergi, A. Erwin, N. Yozbatiran, G. E. Francisco, and M. K. O'Malley, "Design and validation of the ricewrist-s exoskeleton for robotic rehabilitation after incomplete spinal cord injury," *Robotica*, vol. 32, no. 8, pp. 1415–1431, 2014.

[76] L. Dovat, O. Lambercy, R. Gassert, T. Maeder, T. Milner, T. C. Leong, and E. Burdet, "Handcare: a cable-actuated rehabilitation system to train hand function after stroke," *IEEE Transactions on Neural Systems and Rehabilitation Engineering*, vol. 16, no. 6, pp. 582–591, 2008.

[77] J. M. Jacinto-Villegas, O. Portillo-Rodríguez, R. Martinez-Mendez, C. Daza-Merino, A. H. Vilchis-González, and J. C. Avila-Vilchis, "Sistema para control de posición basado en rapid control prototyping (rcp) usando simulink y swb32," *Komputer Sapiens*, vol. 3, p. 11–15, Sep 2019.

[78] J. C. Colado, X. García-Massó, M. Pellicer Catalán, Y. Alakhdar, J. Benavent, and R. Cabeza Ruiz, "A comparison of elastic tubing and isotop resistance exercises," *International journal of sports medicine*, vol. 31, no. 11, pp. 810–817, 2010.

[79] M. Hernandez-Gonzalez and M. Jimenez-Lizarraga, "Real-time laser beam stabilization by sliding mode controllers," *The International Journal of Advanced Manufacturing Technology*, vol. 91, no. 9, pp. 3233–3242, 2017.